BRNO UNIVERSITY OF TECHNOLOGY

VYSOKÉ UČENÍ TECHNICKÉ V BRNĚ

CENTRAL EUROPEAN INSTITUTE OF TECHNOLOGY

STŘEDOEVROPSKÝ TECHNOLOGICKÝ INSTITUT VUT

SINGLE-MOLECULE MAGNETS WITH TRIGONAL SYMMETRY OF THE COORDINATION POLYHEDRON: STRUCTURE, MAGNETIC PROPERTIES AND DEPOSITION ON SURFACES

JEDNOMOLEKULÁRNÍ MAGNETY S TRIGONÁLNÍ SYMETRIÍ KOORDINAČNÍHO POLYEDRU: STRUKTURA, MAGNETICKÉ VLASTNOSTI A DEPOZICE NA POVRCHY

DOCTORAL THESIS

DIZERTAČNÍ PRÁCE

AUTHOR	**Mgr. Lubomír Havlíček**
AUTOR PRÁCE	
SUPERVISOR	**doc. Dr. Ing. Petr Neugebauer, Ph.D.**
ŠKOLITEL	
CO-SUPERVISOR	**Dr. Ing. Ivan Nemec, Ph.D.**
KONZULTANT	

BRNO 2022

Abstract

This thesis focusses on synthesis, structure and magnetization study of Single Ion Magnets with trigonal symmetry and their deposition on surfaces. The first part outlines the introduction into State of the art of the Single Molecule magnets. Followed by description of methods used to perform all discussed characterizations and theoretical background of these methods. In the next part are discussed all the obtained results and it is concluded by discussion about the achieved aims of this thesis. The last part of this thesis provides references and author's published results.

Keywords

Single-Molecule Magnets, Coordination chemistry, Organic chemistry, trigonal symmetry.

Abstrakt

Tato práce se zaměřuje na syntézu, strukturu a magnetické vlastnosti Jedno Iontových Magnetů s trigonální symetrií a jejich depozici na povrchy. První část se zabývá úvodem do tématiky Jedno Molekulových magnetů. Následuje část věnovaná metodám použitým k provedení charakterizací studovaných vzorků, následně je kapitola doplněná o teoretickou část. Dále jsou diskutovány připravené vzorky a následuje diskuze o získaných datech a o dosažení cílů této práce. Závěrečná část obsahuje použitou literaturu a seznam autorových činností v průběhu studia.

Klíčová slova

Jedno Molekulové Magnety, Koordinační chemie, Organická chemie, Trigonální symetrie

I hereby declare that I have written my doctoral thesis topic on the theme SINGLE-MOLECULE MAGNETS WITH TRIGONAL SYMMETRY OF THE COORDINATION POLYHEDRON: STRUCTURE, MAGNETIC PROPERTIES AND DEPOSITION ON SURFACES independently, under the guidance of the thesis supervisor doc. Ing. Petr Neugebauer, PhD. and co-supervisor Ing. Ivan Nemec, PhD., and using literature and other sources of information which are all properly quoted in the thesis and detailed in the list of literature at the end of the thesis.

Contents

List of used abbreviations

SMM – Single Molecule Magnet

SIM – Single Ion Magnet

SCM – Single Chain Magnet

SOC – Spin-orbit Coupling

EPR – Electron Paramagnetic Resonance

PPMS – Physical Properties Measurement System

SQUID – Superconducting Quantum Interference Device

CASSCF – Complete Active Space Self Consistent Field

DFT – Density Function Theorem

XPS – X-ray Photoelectron Spectroscopy

Raman – Raman Spectroscopy

UV/VIS – Ultra-Violet/Visible Light Spectroscopy

IR/FTIR – Infra-Red/Fourier Transform Infra-Red Spectroscopy

SEM – Scanning Electron Microscopy

AFM – Atomic Force Microscopy

XMCD – X-Ray Magnetic Circular Dichroism

EA – Elemental Analysis

XRPD – X-ray Powder Diffraction

VSM – Vibrating Sample Measurement

AC – Alternating Current

DC – Direct Current

SCO – Spin Crossover

ZFS – Zero Field Splitting

QTM – Quantum Tunnelling of Magnetization

MPMS – Magnetic Properties Measurement System

TBY – Trigonal Bipyramid

SPY – Square Pyramid

MOTeS – Magneto-Optical and Terahertz Spectroscopy research group

1. Introduction

Utilization of magnetic phenomena in devices allowed humanity to explore the Earth during the previous centuries. Since that, this research area enormously expanded and due the practical utilization of magnetism in e.g., information and transportation technologies the society profited from unprecedent level of economic globalization based on quantum properties of the nano-world leading to discovery of new kinds of materials with exciting properties. Most of the modern technology, such as transportation, communication, and data storage, is based on the magnetic materials originating in transition and rare-earth metals or their alloys[1]. Nowadays, technological devices' miniaturization and energy efficiency led scientific focus towards materials that can be sufficiently small while preserving their magnetic properties – single-molecule magnets (SMMs). Such molecules exhibit slow relaxation of magnetization of purely molecular origin and are able to preserve direction of its magnetic dipole from changing its orientation due to presence of intrinsic spin-reversal barrier. Such compound is a coordination compound with transition/inner transition ion as a central atom and with spin larger than ½ and axial magnetic anisotropy. The first SMM, famous complex $[Mn_{12}O_{12}(O_2CCH_3)_{16}(H_2O)_4]\cdot 4H_2O\cdot 2CH_3CO_2H$ (abbreviated as Mn_{12}) was synthesized in 1980[2] and its magnetic properties were published more than decade later in 1993[3]. This discovery opened a new field of research and new possibilities for future technology as the first samples showed magnetic hysteresis – an essential phenomenon for creation of magnetic nano-devices. The size on molecular (nm) scale of the newly discovered compounds suggested a potential for significant miniaturisation or great increase in density (in ideal model scenario the area density can reach up to hundreds of thousands of $Tbit/m^2$ compared to current solid-state drives reaching lower thousands of $Tbit/m^2$) of magnetic entities in possible devices[4]. As well as the first SMM (Mn_{12}) also the other new SMMs were based on manganese coordination compounds, which reached very high number of the central atoms. The first iron cobalt based SMM was discovered in 1996[5] expanded the family of SMM by another element and other transition metals based SMM were sure to follow. This was achieved in 2002[6] by discovery of the first cobalt based SMM. Another transition metal SMMs followed (Ni, V, etc.). These first discovered SMMs unfortunately failed to reach desirable magnetic performance at high temperatures. The change came with the discovery of a system containing one lanthanide centre 2003[7], such system gave foundation to new category of SMMs in only one ion centre called Single Ion Magnets (SIMs)[8]. Interesting discovery was achieved in 2012 by preparing iron-based SIM and is described in the beginning of chapter 3.1. This new compound additionally

exhibited spin crossover (SCO) phenomenon allowing it to exist in two spin states with the possibility of switching in between them. Such a combination of phenomena promises a great potential for magnetic and optical sensors or for switchable magnetic devices. Next important milestone was set by discovery of two organometallic SIMs containing Dy(III) centre. The first one was published in 2016 and it pushed the blocking temperature up to 60 K. In 2018, this great discovery was followed by report on its derivate with the blocking temperature increased up to 80 K (these milestones are more discussed in the final part of chapter 3.1), which is above the boiling point of the liquid nitrogen. These results brought the whole research of SMMs closer to application in real life and to forefront of current research with various possible applications as high-density data storage, quantum bits, and molecular spintronics[9,10].

The new challenge for scientists is to create real life devices. To achieve this, it is necessary to have control over the respective molecules. To gain such control, the SIMs have to be deposited on functional surfaces capable e.g. to conduct electric current. This important topic is discussed in the chapter 3.2 of this thesis. The successful deposition could be a challenging due to a need for balance between rational design of the molecules (ligand field symmetry, capability to attach to the surface or to self-assembly on the surface), their physical properties (solubility, sublimation temperature or thermal stability) and deposition techniques. Moreover, the magnetic properties of deposited SMMs/SIMs can greatly differ from a bulk material as their geometry and intra/intermolecular interactions can be significantly modified upon deposition. Carefully designed organic ligands allow coordination of ion and interactions with the substrate via chemical bonds (e.g. S-Au) or via weaker non-covalent interactions (e.g. π-π) to form self-assembled SIMs as hybrid materials devices. Some of the newly prepared hybrid materials show slow relaxation of magnetization with record blocking temperature of 28 K[11]. This field of study is highly uncharted, and carries a great potential for further discoveries.

2. Aims of thesis

Aim of this thesis was to prepare various coordination compounds with trigonal symmetry of their coordination polyhedral, study their crystal structure, investigate their magnetic properties with various techniques (PPMS, SQUID, EPR) and to characterize them as Single Ion Magnets. Selected SIMs with suitable structural and magnetic parameters would be deposited on surfaces such as graphene, gold, silicon or transition metal dichalcogenides. This hybrid materials would be characterized by XPS, Raman spectroscopy, SEM and HF-EPR.

1. The first objective was to prepare coordination compounds with Co(II) and additionally Dy(III). The aim was to synthetize or search for available organic ligands, perform series of chemical reactions and grow high quality single crystals of obtained coordination compounds. Upon design successful synthesis experiments and obtaining crystals this compounds were elementally (XPS, EA), spectroscopically (IR, Raman, UV/VIS) and structurally studied (XRPD, Single crystal X-Ray diffraction).

2. The second objective was to study the magnetic parameters of coordination compounds prepared in Objective 1 and to characterize them as SMMs/SIMs. To complete this objective samples were by VSM in form of powder sample under high magnetic fields and low temperature to obtain information about magnetic susceptibility of prepared samples. VSM was followed by HF-EPR measurements to fine tune the previously gathered magnetic data. These measurements were complemented by theoretical calculations providing complex insight into the studied magnetic properties.

3. The third objective was to deposit selected coordination compounds on various surfaces mainly by thermal deposition using custom-made Sublimation chamber followed by analysis of created hybrid material by SEM, Raman spectroscopy and XPS. The substrates with surfaces were modelled to fit the HF-EPR sample holder so the magnetic properties of such hybrid materials could be studied and compared to bulk materials.

3. State of the Art of Magnetism of Coordination Compounds

This chapter is introduction to the research of molecular magnetism with special attention dedicated to Single Molecule Magnets, which are coordination compounds of the transition or inner transition metals. The chapter aims to briefly introduce history of SMMs and to highlight the most important milestones in this field with major focus on coordination compounds of Dy(III) and Co(II) with trigonal symmetry of ligands or ligand field. This chapter also briefly discuss methodology used for characterization of these compounds. In the end of this chapter the previously reported results on depositions of SMMs on various surfaces (with focus on graphene) are discussed.

3.1 Magnetic materials and Single Molecule Magnets

First, the scientists focused on the synthesis of coordination compounds with high S and several Zero-field SMMs were indeed prepared [18,19,21]. Systems as Mn_{12} have not brought expected results and attempts focused on 3d-4f systems. Several of them were prepared – $[Dy_3Cu_6L_6(\mu_3\text{-}OH)_6(H_2O)_{10}]$[18], $[Ni(\mu\text{-}L)(\mu\text{-}OAc)Dy(NO_3)_2]$[27], $[\{FeF_3(Me_3tacn)\}_2Gd_3F_2(NO_3)_7(H_2O)(CH_3CN)]\cdot 4CH_3CN$[28], $[Mn_{21}DyO_{20}(OH)_2(ButCO_2)_{20}(HCO_2)_4(NO_3)_3(H_2O)_7]$[29] which in the year 2011 created new record for blocking temperature at 77 K, other examples followed[21,23,24,30–33].

The first of 3d row-based SIMs was $[Co(ppc)_4(SCN)_2]$ where ppc = (4-pyridyl)phenylcarbene published in 2003 by Karasawa et al. [25] It possesses coordination number 6. It is necessary to mention that the crystal structure containing carbene ligands was not successfully obtained and the magnetic properties do not come purely from Co(II), but also from other interactions with the carbene unpaired electrons. This octahedral compound consists of cobalt in oxidation state 2+ coordinated by six nitrogen atoms, four coming from ppc ligands, and two from thiocyanate, the crystal structure is available only for precursor $[Co(dpp)_4(SCN)_2]$ where dpp = (α-diazobenzyl)pyridine. The dynamic magnetic measurements revealed two peaks at each frequency and especially at 1 Hz, this suggested the presence of two components A and B. Relaxation time $\tau_0 = 2.3\cdot 10^{-10}$s for component A and $3.2\cdot 10^{-10}$s for component B was obtained from Arrhenius plot. Energy barrier was determined to be $U_{eff} = 89$ cm^{-1}. Blocking temperature was below 3.5 K. The DC magnetic properties show a narrow magnetic hysteresis in the range from 1.9-3.4 K.

Another record for the 3d SIMs family was reported by Zadrozny et al. in 2011 and it was coordination compound $(Ph_4P)_2[Co(SPh)_4]$ [34]. Complex anion is a simple molecule with coordination number 4 and an approximate D_{2d} symmetry, which exhibited remarkable

magnetic relaxation in zero applied magnetic field. Authors assumed that quantum tunnelling is possible thanks to the mixing of $\pm Ms$ spin states via hyperfine interaction, dipolar interaction. Due to a large separation between molecules and utilization a non-integer spin, the mixing of spin states by E is prohibited by Kramer's theorem.

In DC magnetic measurements the value of effective magnetic moment start to decrease at 80 K. The best fit of DC magnetic data afforded $D = $ -74 cm^{-1}. Frequency dependent AC measurement shows temperature dependent peaks appearing from 1.8 K to 7 K when the frequency limit of the magnetometer was reached. This compound is a zero-field SIM, but the application of small external field significantly improves AC data.

This compound was diluted by isostructural compound (Ph$_4$P)$_2$[Zn(SPh)$_4$] to study intermolecular interactions and their influence on the magnetic properties. The dynamic magnetic behaviour under zero and applied field is different in this case, the maxima are shifted to lower frequency instead of forming another peak. Arrhenius plot showed temperature independence in contrast with a temperature-dependent plot in case of application of an external field or dilution with zinc. Energy barrier was determined to be $U_{eff} = 21$ cm^{-1} (relaxation time τ_0 = 1.0·10^{-7} s), which is in contrast a value predicted by EPR was $U_{eff} = 140$ cm^{-1}.

(Ph$_4$P)$_2$[Co(SPh)$_4$] was followed by other two related compounds (Ph$_4$P)$_2$[Co(OPh)$_4$] and (Ph$_4$P)$_2$[Co(SePh)$_4$] by Zadrozny in 2013 [35]. Although published compound (Ph$_4$P)$_2$[Co(OPh)$_4$] is not zero field SIM its diluted form K(Ph$_4$P)[Co$_{0.06}$Zn$_{0.94}$(OPh)$_4$] is. The symmetry of (Ph$_4$P)$_2$[Co(OPh)$_4$] is C_1 due to significantly twisted geometry of the phenyl ligands. After substitution of Ph$_4$P$^+$ by K$^+$ cation the symmetry has changed to D_{2d} due to the K$^+\cdots$O interactions (**Figure 1**).
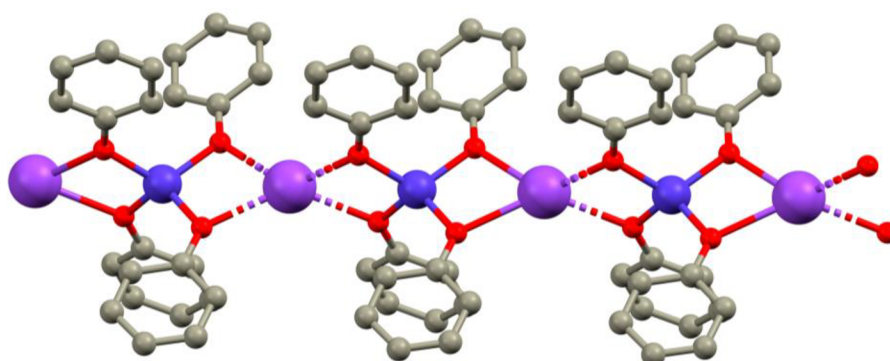
Figure 1: A perspective view on K$^+\cdots$O interaction in K[Co(OPh)$_4$]

DC magnetic measurements showed a decrease of magnetic moment starting at 100 K. The DC data were fitted to spin Hamiltonian to obtain D and E parameters, which resulted in $D = $ -83 cm^{-1} for (Ph$_4$P)$_2$[Co(SePh)$_4$]. AC measurements showed slow relaxation of magnetization at 2

K under zero applied field. Arrhenius plot corresponds to Orbach relaxation whereas Raman relaxation produces deviations from the plot. The values of dynamic parameters were obtained for K(Ph$_4$P)[Co$_{0.06}$Zn$_{0.94}$(OPh)$_4$], U_{eff} = 34 cm^{-1} and τ_0 = 1.0·10^{-9} s and for (Ph$_4$P)$_2$[Co(SePh)$_4$], U_{eff} = 19 cm^{-1} and τ_0 = 3.0·10^{-6} s. The dipolar interactions of cobalt ions is partially responsible for lower barrier values than in the non-diluted compound.

Decrease of magnetic moment in DC magnetic measurements decreases at 120 K down to 1.8 K, which is typical dependence for tetrahedral cobalt-based SIMs. Data were analyzed using spin Hamiltonian and fitted to D = -161 cm^{-1} and zero rhombicity. From AC measurements a maximum at 2 K and 0.84 Hz is observable which rapidly shifts to higher frequencies with increasing temperature. Arrhenius plot is not linear in the whole range suggesting other types of relaxation giving values of U_{eff} = 33.9 cm^{-1} and τ_0 = 4.5·10^{-6} s. The fit of barrier and relaxation type was changed only very little by application of an external field or dilution by diamagnetic zinc ion. Even after the application of a very high magnetic field of 45 T was not possible to obtain EPR spectra.

Another zero-field SIM is compound [Co(paz)$_3$(PhB)]Cl, where paz = tris-pyrazolooximate and PhB = phenylboronic acid, with coordination number 6 and trigonal prismatic geometry. This was prepared for the first time by Varzatskii et al. in 2014 and magnetism was studied by Novikov et al. in 2015 [39,40]. DC measurements in a broad range of temperatures showed a gradual decrease of effective magnetic moment upon decreasing temperature, which indicate large magnetic anisotropy. Using spin Hamiltonian the D and E parameters were fitted to obtain D = -82 cm^{-1} and E/D = 0.003, indicating thus very large and axial anisotropy. No magnetic hysteresis was observed. Analysis of NMR spectra of [Co(paz)$_3$(PhB)]Cl via van Vleck equation was done to obtain D = -109 cm^{-1}, which is very similar to DC experiment and CASSCF calculations (D = -110 cm^{-1}, E/D = 0.004). Arrhenius plot shows non-linear dependence of relaxation time at temperature and significant deviation at higher temperatures. The value of the energy barrier was calculated to be U_{eff} = 102 cm^{-1}. A magnetic hysteresis was observed for this compound.

In the year 2015, a compound [Co((NtBu)$_3$SMe)$_2$] was published by Carl et al.[41] According to the X-ray experiment, this molecule has coordination number 4 and C_{2v} symmetry due to a distorted tetrahedral geometry of coordination polyhedron. The structure of bulky peripheral ligands secure that the cobalt ions are magnetically well isolated. The fit of DC magnetic data on spin Hamiltonian provided D = -58 cm^{-1} and E/D = 0.15. From the Cole-Cole diagram and Arrhenius plot, the values of U_{eff} = 75 cm^{-1} and τ_0 = 2.64·10^{-8} s were obtained.

In 2015 published Shao et al. [42] how anisotropy of trigonal Co(II) coordination compounds can be tuned by exchange of the donor atoms. The authors prepared two compounds. First [Co(Me$_6$tren)Cl](ClO$_4$) with tetradentate ligand, where all the donor atoms of the organic ligand are nitrogen atoms. Second compound was [Co(NS$_3^{iPr}$)Cl](BPh$_4$) with the same shape of coordination sphere (trigonal bipyramid with pseudo-C_{3v} symmetry) as the first type and also very similar tetradentate ligand, but with one axial nitrogen and three equatorial sulfur and donor atoms. DC and AC measurements were performed confirming SIM behavior. By the exchange of the donor atoms (S for N), the authors managed to increase the energy barrier from 16 cm^{-1} to 32 cm^{-1}. From magnetization measurements a magnetic hysteresis was observable for [Co(NS$_3^{iPr}$)Cl](BPh$_4$).

A cobalt-based SIM of mixed valence (HNEt$_3$)(Co(II)Co(III)$_3$L$_6$) was reported by Zhu et al. in 2013 [45]. According to the X-Ray experiment the coordination number of a central atom Co(II) is 6 and is coordinated by six oxygen donor atoms which gives it geometry of slightly distorted trigonal prism of D_3 symmetry. The central atoms Co(III) also possess coordination number 6 with four oxygen donor atoms and two nitrogen donor atoms. The DC magnetic measurements give the ZFS parameters: D = -115 cm^{-1}, E = 2.8 cm^{-1} and g = 3.05. The AC magnetic measurements revealed presence of slow relaxation of magnetization even without the presence of external magnetic field and confirmed this compounds as zero-field SMM.

Many lanthanide-based SIMs have been prepared since discovery of first Ln based SIMs. Since this thesis is focused on SIMs with trigonal symmetry it is appropriate to discuss several examples of lanthanide-based zero-field SIMs with such symmetry.

Several Dy(III) compounds with simple trigonal aliphatic ligand H$_3$tea = triethanolamine were published. [Dy$_2$(NO$_3$)$_4$(teaH$_2$)$_2$] was reported in 2017 by Margaritis et al. [49]. The symmetry of the complex is close to D_{2h}. Each Dy(III) atom has coordination number 9 atom is coordinated by one tetradentate H$_3$tea ligand and two NO$_3^-$ ligands, each Dy is additionally coordinated by and O-donor atom from neighboring H$_3$tea. The AC magnetic measurements unfortunately did not revealed a slow relaxation of magnetization.

Another dimer [Dy$_2$(teaH$_3$)$_2$(MeCOO)$_4$] was published in 2018 by Koroteev et al. [50]. In the complex molecule each the Dy(III) atom has coordination number 8 due to coordination of the central atom by tetradentate H$_3$tea and by one monodentate MeCOO$^-$ ligand. The geometry of coordination polyhedron is distorted trigonal dodecahedron. The DC magnetic measurements

showed a sharp decrease of the effective magnetic moment below 6 K but AC magnetic measurements were not performed.

3.2 Depositions of Single Molecule Magnets

To construct spintronics or data storage devices out of SMM/SIMs, it is necessary to create organized molecular arrays and to have a control over the individual molecules. One of the possible ways is to make addressable layers by deposition on the surfaces. This caused rising interest in fabrication and utilization of so-called 2D materials. The most studied is graphene, a single layer of the carbon atoms in hexagonal arrangement with interesting chemical and electrical properties that hold promise for a next generation of electronic devices. The goal is to combine 2D materials with well-designed SMMs and create hybrid materials with the defined layer of the SMMs molecules on the selected surface. The deposition can be strengthened by forming the covalent bonds between SIM/SMM and the surface (for example Au-S covalent bonds). For organized deposition of SMM on graphene the non-covalent interactions – alky-π, π-π, or halogen-π play a significant role. Coordination compounds with long alkyl chains or aromatic rings will then form such interactions with graphene and self-assemble on a surface [59,60]. Ligands containing halogens can interact with graphene-based surfaces due to halogen electronegativity and affect the electronic transport in graphene, and thus magnetic properties of the prepared hybrid material [61]. Most of the reported results are based on phthalocyanine ligands forming a uniform layer as these compounds are planar and aromatic. These reports show that the magnetic moment of deposited SIMs remained unquenched, and thus these systems are good candidates for spintronics [62,63]. More variability in the type of the central atom and shape of the coordination sphere, crucial for magnetic properties, is offered by SIMs with the ligand in the shape of aromatic anchoring arms – such chemical modification offers a way for SIM/SMM to interact with a surface.

For the first time a magnetic hysteresis of the SMM deposited in a form of monolayer was observed in 2010 by Mannini et al[64]. Mannini took and advantage of chemical modification of already known Fe4 based SMM compound and prepared [$Fe_4(L)_2(DPM)_6$] (where H_3L is 7-(acetylthio)-2,2-bis(hydroxymethyl)heptan-1-ol and HDPM is dipivaloylmethane) in which the long aliphatic chain is terminated by the sulfur atoms. Molecules of this compound were deposited onto a gold surface as gold and sulfur has strong affinity and form together strong Au-S bonds. The magnetic hysteresis of such created hybrid material was studied by XMCD which directly proved that the easy magnetization axis of the deposited complex molecule were

oriented perpendicular to the surface. The magnetic properties have remained unchanged in comparison with the bulk material.

The properties of SMM/SIMs can change in combination with surfaces. Such a change can be positive as was reported by Wäckerlin et al. in 2016 [65] where authors deposited [TbPc$_2$], where Pc = phthalocyanine, on nonmagnetic and insulating MgO surface on Ag. The SIM molecules were adsorbed on the surface by sublimation and scanning tunnelling microscopy revealed that they self-assembled themselves into the perfect 2D islands. This excluded the possibility of a magnetic contribution of the [TbPc$_2$] molecules tilted towards the surface. The XMCD revealed significant widening of magnetic hysteresis compared to the bulk material. Thermally dependent XMCD showed slow relaxation of magnetization bellow 8 K. The best results were obtained upon deposition on multilayer of MgO, even though that [TbPc$_2$] deposited on MgO monolayer still showed magnetic hysteresis. It was found out that upon deposition the [TbPc$_2$] retains its almost prefect D_{4d} symmetry, which contrasts with breaking symmetry of [TbPc$_2$] to C_{4v} and lower, upon its deposition on the metallic surfaces (such systems showed almost no or no hysteresis)[66,67].

The magnetic properties can also worsen or even be suppressed upon deposition of SMMS on a surface. Bogani et al. published in 2007 a deposition of [Mn$_{12}$O$_{12}$(pCH$_3$SC$_6$H$_4$COO)$_{16}$(H$_2$O)$_4$] on the gold surface. The SMM was anchored to the surface in a form of monolayer by strong Au-S bonds. This hybrid material was studied by magnetic molecular dichroism and the absence of magnetic hysteresis was revealed suggesting dramatic change in magnetic properties upon deposition. Mannini et al. published deposition of [Mn$_{12}$O$_{12}$(RCO$_2$H)$_{16}$(H$_2$O)$_4$]·4H$_2$O·2CH$_3$CO$_2$H (where RCO$_2$H = 4-(methylthio)benzoic acid) on a gold surface in 2009. In this case the Mn$_{12}$ molecules were simply adsorbed on the surface as there is no anchoring functional group which could form a bond with the gold surface. The sample was deposited in form of few hundred nanometers thick film and was not investigated in more detail. The successful deposition was confirmed by X-ray absorption spectra. The XMCD and μ-SQUID measurements showed no indication of slow relaxation of magnetization and thus, the SMM properties of bulk material were quenched by the deposition [68].

L. Spree et al published chemically derivatized Tb$_2$@C$_{80}$(CH$_2$Ph) SMM where a pyrene function group served as an anchor for deposition on a graphene and graphite surface by forming π-π interaction between pyrene and the surface[11]. The comparison of magnetic hysteresis (obtained by XMCD) for bulk and hybrid material showed only slight worsening of

the magnetic properties upon deposition and the hybrid material still showed magnetic hysteresis. The blocking temperature of the hybrid material was 28 K and for the bulk 29 K. The AFM showed thickness of the hybrid material to be 1.8-2 nm.

4. Obtained Results

List of used Experimental Methods

Structural analysis: The crystal structures were obtained using X-ray diffractometer XtaLAB Synergy-i (Rigaku) with micro focused X-ray source PhotonJet-i (Cu) and detector HyPix Bantam. The powder diffraction data were obtained using XRPD MiniFlex600 (Rigaku, Tokyo, Japan).

Magnetic measurements: Data for **2b** and **3d** were obtained using VSM Cryogenic Limited Magnetometer (Cryogenic Limited, London, UK). The temperature and field-dependent magnetic data were studied as finely grinded powder dispersed in eicosane and fixed in a plastic straw. Data of the remaining samples were obtained using PPMS Quantum Design (Quantum Design Inc., San Diego, CA, USA). The temperature and field-dependent magnetic data were studied as finely grinded powder samples pressed into QD capsule. The AC data for **3d** were obtained using MPMS XL7 SQUID magnetometer (Quantum Design Inc., San Diego, CA, USA). The obtained magnetic data were analysed by EasySpin[77] a module for Matlab and fitted to Spin Hamiltonian. The data for **1a** were analysed using Poly_Aniso software[78–80].

HF-EPR measurements: HF-EPR data were collected using Frascan spectrometer (MOTeS research group, CEITEC BUT, Brno, Czech Republic). The data were analysed by EasySpin[77] a module for Matlab and fitted to Spin Hamiltonian.

Theoretical calculations: The magnetic exchange was investigated by DFT calculations (Broken Symmetry DFT). The ZFS parameters have been calculated using CASSCF/NEVPT2 which were utilised to calculate all energy levels resulting from $3d^7$ electronic configuration with the ORCA 4.2 computational package[81,82]. The ab initio ligand field theory (AILFT) was used to calculate the splitting of d-orbitals[83].

Spectroscopy: The XPS spectra have been collected with X-ray Photoelectron Spectroscopy Axis Supra (KRATOS-XPS) (Kratos, Manchester, UK) and Raman spectra with IR Raman Bruker RFS 100 (IR-RAMAN) (Bruker, Billerica, Massachusetts, USA). The data were analyzed using CasaXPS software [84].

5.1   Dy(III) Coordination Compounds

As was discussed in chapter 3.1, SMM/SIM of Dy(III) with Mannich type of ligands are uncharted territory. Moreover, this type of the ligands impose trigonal symmetry, which can be used in preparation of less common coordination numbers (e.g. 6 or 7) if the ligands contain sterically demanding substituents (e.g. $-CH(CH_3)_2$, $-C(CH_3)_3$,).

For this thesis a series of organic ligands were prepared via Mannich reaction and eight of them were successfully isolated (**Figure 2**). It was intended to prepare tetradentate ligands

with either three O-donor and one N-donor atom or two O-donor and two N-donor atoms. For these structural reasons were chosen also reactants such as glycine, 2-picolylamine and 4-picolylamine and were reacted with formaldehyde and various derivates of phenol. It was expected that upon reaction with dysprosium salts complex the precursor complexes with the coordination number 8 or 9 will be formed as Mannich ligand provides four coordination bonds and NO_3^- or solvent ligands may provide up to four coordination bonds. The syntheses of the following complexes were attempted, the expected compositions are outlined here, although the possible dimerization and other combinations (protonation *vs.* presence of the NO_3^- and solvent ligands) cannot be excluded: [Dy(LX)(HLX)], [Dy(HLX)(NO₃)₂], [Dy(LX)(solv)₂₋₃] (where H₃LX = is one of the prepared Mannich ligands). Such compounds could be further used after introduction of appropriate bi- or tridentate blocking ligand (e.g. 2,2'-bipyridine-N-oxide, or tridentate Schiff base ligands originating from condensation of salicylaldehyde derivatives and ortho-aminophenols) for synthesis of the target six or seven coordinate Ln complexes. Even though that many attempts to synthesize coordination compounds with the H₃LX ligands were performed, including extensive screenings of the different basicity (Dy:base from 1:0 up to 1:10) and reactant ratios (Dy:H₃LX from 1:1 up to 1:4), the chemical identification of the prepared products was never successful. Also, various hydrothermal reaction conditions were tested, but the performed reactions did not bring any success and typically resulted in forming insoluble white powder product. Characterization of such powders never led to the confirmation of the chemical identity.

Following these attempts, the rather complex ligands were replaced by simpler trigonal ligand triisopropylamine (H₃tipa). H₃tipa possesses trigonal structure and three O-donor and one N-donor ligand which is suitable for coordination of Dy(III). As shown in chapter 3.1 coordination of simple trigonal aliphatic ligands to Dy(III) usually lead to coordination number 9. Extensive series of reactions of H₃tipa and Dy(III) salts with varying ration of used base to modify the deprotonation of the H3tipa were performed in attempt to prepare – [Dy(H₂tipa)₂Cl], [Dy(H₂tipa)(Htipa)], [Dy(H₂tipa)(Htipa)(NO₃)], [Dy(tipa)(NO₃)₂]. The attempts were unsuccessful or resulted in isolation of dimeric coordination compound [Dy₂(Htipa)₂(NO₃)₄]·2Et₂O – **1a**.
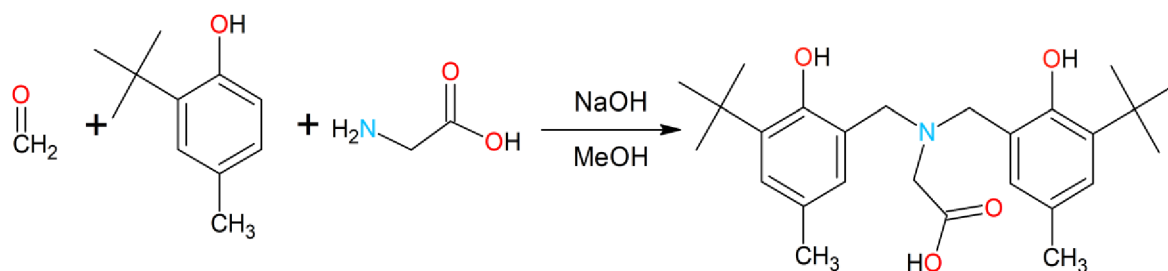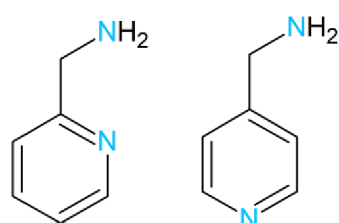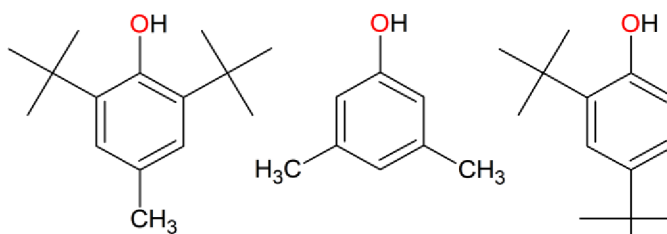
Figure 2: (a) chemical synthesis of mannich type ligand. (b) glycin was replaced by 2-picolylamine and 4-picolylamine. (c) 2-tert-butyl-4-methylphenol was replaced by 2,6.di-tert-butyl-4-methylphenol, 3,5-dimethylphenol and 2,4-di-tert-butylphenol.

Synthesis of $[Dy_2(Htipa)_2(NO_3)_4] \cdot 2Et_2O$ (**1a**) was done as follows: 1 mmol of $Dy(NO_3)_3 \cdot 7H_2O$ was dissolved in 5 ml of MeOH and it was mixed with a solution of 2 mmol of H_3tipa in 10 mmol of MeOH. This solution was stirred at room temperature for 24 hours, filtered with paper filter and crystalized by slow diffusion of diethylether. Colorless crystals formed after two weeks.

Crystal structure:

Complex $[Dy_2(Htipa)_2(NO_3)_4] \cdot 2Et_2O$ crystallizes in the $P2_1/n$ space group. Both Dy(III) central atoms are coordinated each by one tetradentate ligand H_3tipa forming metal-ligand (ML) bond lengths between the central atom and one nitrogen (d(Dy-N) = 2.596(3) Å) and three oxygen (d(Dy-O) = 2.278(2), 2.405(2), 2.408(2) Å) donor atoms. The H_3tipa ligand function also as the bridging ligand in the dimer as each Dy is coordinated by one oxygen atom from the adjacent H_3tipa ligand (d(Dy-O) = 2.244(2) Å). Additionally, each Dy is coordinated by two nitrate ligands in a bidentate manner (d(Dy-O) = 2.488(2), 2.495(2), 2.503(2), 2.521(2) Å) (**Figure 3**). The intramolecular Dy⋯Dy distance is 3.709(3) Å.

The unit cell contains two diethylether molecules per complex molecule, which is stabilized in the crystal structure by hydrogen bond formed between the oxygen atom from diethylether and hydroxy group of Htipa (d(O⋯H-O) = 2.727(3) Å).
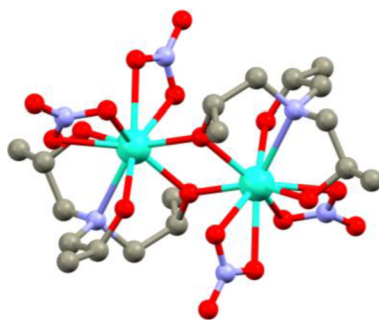
16

Figure 2: Crystal structure of [Dy₂(Htipa)₂(NO₃)₄]·2Et₂O. Grey (C), light blue (N), azure (Dy), red (O).

<u>Magnetic properties and Theoretical calculations:</u>

The effective magnetic moment (μ_{eff}/μ_B) is significantly decreasing with decreasing temperature from about 30.71 at 300 K down to 32.33 at approximately 20 K where follows clear and sudden drop of μ_{eff}/μ_B to 15.68 at 2.99 K. These values are expected for Dy(III) dimer SMM (14.17μ_B). Using CASSCF calculation together with fitting the magnetic data the exchange interaction between both central atoms was obtained J = -0.409 cm⁻¹.

Using CASSCF theoretical calculations it was possible to determine the value of spin-reversal barrier for single Dy(III) centre and the probability of relaxation processes. The relatively high probability of QTM suggests that compound **1a** will be field induced SMM (**Figure 4**).
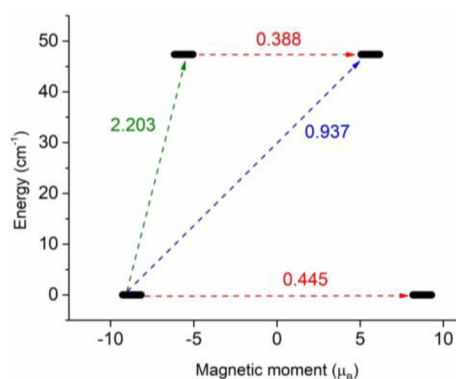
*Figure 4: CASSCF calculation of the spin-reversal barrier of **1a**. Red dashed lines are QTM. Blue dashed line is thermally assisted QTM process and green dashed line is Orbach process of relaxation. The numbers indicate probability.*

5.2   Co (II) SIMs with Tripodal Ligand trenb

The complexes with the ligand trenb (tris(2-aminoethyl)amine) were chosen due to their specific molecular geometry. First, the trenb ligand partially encapsulates the Co(II) central atom and allows coordination of only one additional monodentate ligand, resulting thus in coordination number 5. The geometry of such coordination polyhedron is close to trigonal bipyramidal and such Co(II) complexes have proved to be interesting SIMs[39,40,42]. Next, upon a formation of the complex, three phenyl functional groups form kind of tripodal geometry,

17

which after deposition may be oriented towards the substrate (and can possibly further rotate) enabling formation of the π-π interactions between the substrate (e.g. graphene). Such geometry can help and improve self-assembly distribution of the complex molecules on the surface of substrate [60,62,85–87].

Series of 13 coordination compounds have been synthetized and resynthesized. The crystal structures of two of these compounds have been reported earlier -[Co(trenb)N$_3$]Cl by H. Jiang et al.[88] and [Co(trenb)(NCS)]Cl by Y. Xie et al.[89]. Furthermore, part of a series was partially described in my master's thesis[90]. Herein, this series was fully structurally and magnetically characterized and used for deposition on the selected surfaces with goal to study such hybrid systems by HF-EPR. Four bulk samples have been studied by HF-EPR and the obtained ZFS parameters have been compared with the magnetic measurements and theoretical calculations. Selected samples have been studied by Raman spectroscopy and XPS followed by several attempts for wet and thermal depositions on gold, SiO$_2$ and graphene substrates.

The substrates have been chosen based on the chemical formula of the samples and their geometrical orientation (*vide supra*) given by the crystal structure. The presence of the NCS$^-$ ligand offers a possibility for anchoring the coordination compound on a gold surface due to very high mutual affinity of the gold and sulphur atoms and to create a self-assembly pattern for the samples allowing to control the distribution of SIMs as it is necessary for bottom-up preparation of functional hybrid systems[91–94].

A complete series consists of 13 coordination compounds: [Co(trenb)N$_3$]Cl (**2a**), [Co(trenb)N$_3$]Br (**2b**), [Co(trenb)(NCS)]Cl·MeOH (**2c**), [Co(trenb)(NCS)]Br (**2d**), [Co(trenb)(NCSe)]Cl (**2e**), [Co(trenb)(NCSe)]Br (**2f**), [Co(trenb)(NCO)]Br (**2g**), [Co(trenb)Cl]Cl (**2h**), [Co(trenb)Br]Br (**2i**), [Co(trenb)Cl]Br (**2j**), [Co(trenb)Br]I (**2k**), [Co(trenb)Cl]I (**2l**), [Co(trenb)I]I (**2m**).

Crystal structures:

The crystal structure of samples **2g**-**2j** and **2l** could not be resolved into good publication quality due to low quality of the crystals. Nevertheless, the quality was high enough to confirm coordination sphere and distinguish which halogen atom is coordinated and which remains as a counter ion in the crystal structure.

Compounds **2a**-**2f** are isomorphous and they crystalize in the orthorhombic *P*bca space group. Compound **2j** crystalize in the *P*nma space group, **2k** in *P*6$_5$ space group and **2m** in *P*6$_1$

space group. Compounds **2c** contain crystal solvate methanol. All the complex molecules in **2a-2m** are pentacoordinate with the cobalt(II) central atom. The tetradentate trenb ligand encapsulates the Co(II) atom and forms four Co−N bonds, while the fifth position is occupied by the (pseudo)halido monodentate ligand. The counter anion in the second coordination sphere changes through the series (Cl⁻, Br⁻, I⁻). Three nitrogen donor atoms (N1, N2, N3) are the secondary amines and are located in the equatorial positions. The fourth N-donor atom (N4) is from tertiary amine group located in the axial position. The ML bond lengths with the trenb ligand are very similar for the whole series. The longest ML bonds were observed for the bonds with the halido ligands, the second longest are those with the N4 donor atom: $\underline{d}$(Co-X) = 2.35 − 2.69 Å, d(Co-N4) = 2.21 − 2.23 Å. The Co−N bonds with the equatorial nitrogen atoms are very similar throughout the series and they are the shortest: d(Co-N(1,2,3) = 2.07 − 2.11 Å. The geometry of the coordination polyhedra in **2a-2f** is slightly distorted trigonal bipyramid as can be described by the Addison parameter τ in **Table 1**. The crystal packing in the whole series is organized by the N–H⋯X⋯H–N interaction, which is causing the zig-zag packing, however, the observed donor-acceptor classify the present interactions among the weak non-covalent contacts: d(N⋯X) = 3.29 to 3.63 Å [95](**Figure 5** and **Table 1**). Additionally, in **2a-2d** the C–H⋯N hydrogen bonds between the N₃⁻ or NCS⁻ ligand and the aromatic C–H group of trenb were formed: d(C⋯N) = 3.23 − 3.79 Å.
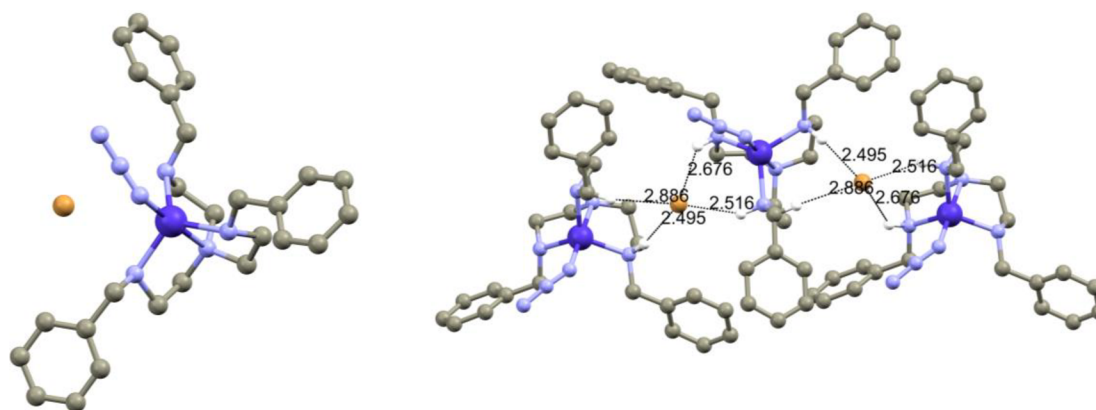
*Figure 5: Depiction of assymetric unit in the crystal structure of **2b** (left). Depiction of the H-Br interactions (black dashed lines) in the crystal lattice of **2b**. Grey (C), light blue (N), purple (Co), brown (Br), white (H). The hydrogen atoms besides those inolved in hydrogen bonding were ommited for clarity. Shown distances are in Å.*

Table 1: Summary of α and β angles, Addison parameter τ and bond lengths in the series of compounds with trenb ligand and showing average distance of hydrogen bonds between N-H⋯X⋯H-N.* single crystal data are of bad quality.

	τ	N1	N2	N3	N4	N5/X	N⋯X⋯N

2a	0.95	2.095(3)	2.091(3)	2.087(3)	2.226(1)	2.219(4)	3.301(2)
2b	0.99	2.095(4)	2.098(5)	2.115(5)	2.227(5)	2.010(5)	3.437(1)
2c	0.91	2.079(2)	2.097(2)	2.090(2)	2.218(2)	2.034(2)	3.289(2)
2d	0.91	2.107(3)	2.090(3)	2.092(3)	2.216(3)	2.051(3)	3.426(3)
2e	0.93	2.069(5)	2.088(5)	2.084(5)	2.216(5)	2.045(5)	3.305(4)
2f	0.93	2.081(3)	2.107(3)	2.096(3)	2.209(3)	2.081(3)	3.426(1)
2i	0.90	2.101(2)	2.119(2)	2.101(2)	2.225(2)	2.467(5)	3.414(3)
2j*	0.98	2.076	2.088	2.088	2.191	2.352	3.629
2k	0.96	2.084(6)	2.089(5)	2.102(5)	2.221(5)	2.496(1)	–
2m	0.91	2.089(8)	2.096(1)	2.121(9)	2.207(1)	2.687(2)	–

Magnetic properties:

Compounds **2a**-**2m** follow very similar behavior in both temperature and field dependent measurements. The μ_{eff}/μ_B is decreasing with decreasing temperature from about 4.5 at 300 K down to 4.2 at approximately 20 K, sudden drop of the μ_{eff}/μ_B value occurs (below 4.0 at 1.8 K). Such magnetic behavior is are typical for Co(II) SIMs as it demonstrates occurrence of ZFS. Magnetic measurements were newly performed and analyzed for **2b**. The temperature dependent data follow the same pattern as previously described for the rest of the series. The magnetic data have been fitted to the ZFS spin Hamiltonian) and the found ZFS parameters are D = -5.39 cm^{-1}, E/D = 0.17, g_{iso} = 2.24. Thus, the magnetic anisotropy of **2b** is small and axial, but with relatively large rhombicity.

HF-EPR:

The compounds **2a**, **2d**, **2f**, **2j** have been studied by HF-EPR. The ZFS parameters (zero-field resonance) for the **2a** (375 GHz) and **2j** (420 GHz) were directly observed in the HF-EPR spectra. The collected data have been fitted and the results of these analysis give important comparison with data obtained after analysis of PPMS measurements and theoretical calculations (**Table 2**). Additionally, the anisotropic g-values have been fitted. It is noteworthy to mention that the very large broadening of signals in the spectra of **2j** is caused by the exchange interactions in the crystal structure as the Co(II) centres lie relatively close to each other $d(Co \cdots Co) = 6.490$ Å and in the plane of Co$\cdots$Co interaction lies the chlorido ligand $d(Co \cdots Cl) = 4.145$ Å and his hydrogen bonds with ligand trenb as described in structure of **2j**. The ZFS parameters obtained by fitting of EPR data are not in all cases in a good agreement with the values found by magnetic measurements. In the case of the small values of magnetic anisotropy in **2f** and **2d** (**Table 2**) the mismatch between the D signs determined by EPR and magnetometry is not surprising, because the fitting of the latter is not capable to distinguish correct sign of small D (e.g. with magnitude comparable to 2 cm^{-1}), especially in the case when rhombicity is present and fit was done for isotropic g-value. For **2j**, the $|D|$ value is still in reasonable agreement, however, the analysis of the EPR spectra was strongly affected by the line broadening. The relatively large difference between the calculated and experimentally (both magnetometry and HFEPR) determined D parameter in **2d** is hard to explain without a great deal of speculation. However, it must be emphasized that the temperature at which the crystal structure (and thus input geometry for calculations) was determined was much larger (150K) in comparison to the temperature range at which HFEPR was measured and at which the magnetic properties are sensitive to the present ZFS (below 20 K).

*Table 2: Comparison of the ZFS parameters obtained from DC measurements, from HF-EPR and from CASSCF/NEVPT2 calculations for 2a, 2d, 2f and 2j. * g values obtained from PPMS are g_{iso} only.*

[Co(trenb)(N$_3$)]Cl **2a**	D	E/D	g_x	g_y	g_z
PPMS	-5.6	–		2.24*	
HF-EPR	-6.2	0.08	2.0	2.3	2.3
CASSCF	-2.3	0.09	2.2	2.2	2.3
[Co(trenb)(NCS)]Br **2d**	D	E/D	g_x	g_y	g_z
PPMS	-1.80	0.00		2.26*	
HF-EPR	2.14	0.16	2.15	2.09	2.24
CASSCF	-7.13	0.09	2.23	2.24	2.39

[Co(trenb)(NCSe)]Cl **2f**	D	E/D	g_x	g_y	g_z
PPMS	1.90	0.06		2.19*	
HF-EPR	-1.6	0.25	2.16	2.21	2.23
CASSCF	-4.6	0.14	2.19	2.27	2.22
[Co(trenb)Cl]Br **2j**	D	E/D	g_x	g_y	g_z
PPMS	-4.5	0.03		2.19*	
HF-EPR	8.5	0.05	2.1	2.3	2.2
CASSCF			–		

Theoretical calculation:

The CASSCF/NEVPT2 calculations were performed to theoretically predict the values of the ZFS and ligand field parameters (AI-LFT procedure). The summary of the calculated ZFS parameters for the trenb series can be found in **Table 3**.

Table 3: Summary of ZFS parameters of 2a, 2b, 2c, 2d, 2e and 2f obtained from theoretical calculations

	D	E/D	g_x	g_y	g_z
2a	-2.30	0.09	2.2	2.2	2.3
2b	-16.88	0.02	2.22	2.23	2.43
2d	-7.13	0.09	2.23	2.24	2.39
2e	1.27	0.25	2.24	2.25	2.36
2f	-4.60	0.14	2.19	2.27	2.22
2k	-4.02	0.13	2.25	2.27	2.36
2m	4.96	0.10	2.25	2.31	2.35

In general, the magnetic anisotropy is small with the D parameters adopting both positive and negative values, and rhombicity is significant. This can be explained on basis of the calculated electronic structure. First, the splitting of the ^4F atomic term to ligand field terms (LFTs) resulted in first excited LFT being energetically well separated from the ground state for 4000 cm^{-1} or even more (**Figure 6**). Next, the splitting of the d-orbitals corresponds well with expectations for the trigonal bipyramidal geometry with the degenerate pairs of d_{yz}, d_{xz} and d_{xy}, $d_{x^2-y^2}$ orbitals and (lowest in the energy), and d_{z^2} having the highest energy. Orbitals d_{yz} and d_{xz} are both occupied by two electrons, d_{xy}, $d_{x^2-y^2}$ and d_{z^2} is occupied with one electron each (**Figure 6**).Since the orbitals d_{xy} and $d_{x^2-y^2}$ have identical shape and the same quantum number ($m_l = \pm2$) and the orbitals superimposable by rotation about an axis so the orbital angular momentum is present [96].
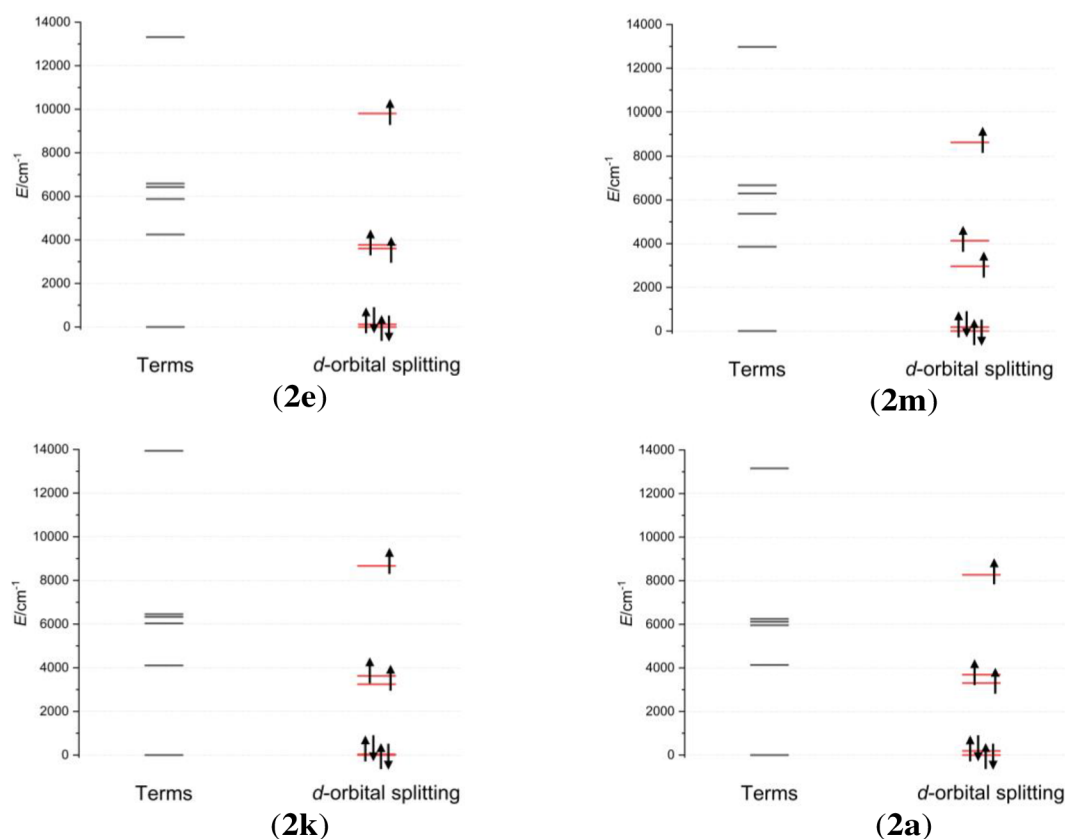
*Figure 6: Graphical representation of the ligand field terms and d-orbital energy levels as calculated by CASSCF/NEVPT2 for complexes **2a**, **2e**, **2k** and **2m**.*

Depositions:

Coordination compounds in this series have suitable ligands for deposition on the surfaces such as gold and graphene. Due to very poor solubility of **2a-2m** in any solvent a thermal sublimation was attempted. 15 nm thick film on the graphene and gold substrate was sublimed (at 350 °C). To verify the intactness of the studied compound, Raman spectroscopy was performed to compare the vibrational modes of the individual components of the resulting hybrid material. **Figure 7** shows Raman spectra, from top to bottom, of a SiO_2/Si + CVD graphene, powder of **2a** and deposited **2a** by thermal sublimation. The Raman spectrum of the bulk compound **2a** contains peaks characteristic of the ligand's functional groups such as benzyl, amine, and azide [97,98]. The strongest peaks around 1000, 1600, 3000 cm^{-1} originated mainly from benzyl group. In the Raman spectrum of the sublimated sample, we also observed these peaks, but their relative ratios were different. The peak around 1000 cm^{-1} was no longer the strongest and peaks around 3000 cm^{-1} were dominated by aliphatic C-H bonds (< 3000 cm^{-1}) over aromatic (>3000 cm^{-1}). This indicated that compound **2a** has underwent a change during deposition.
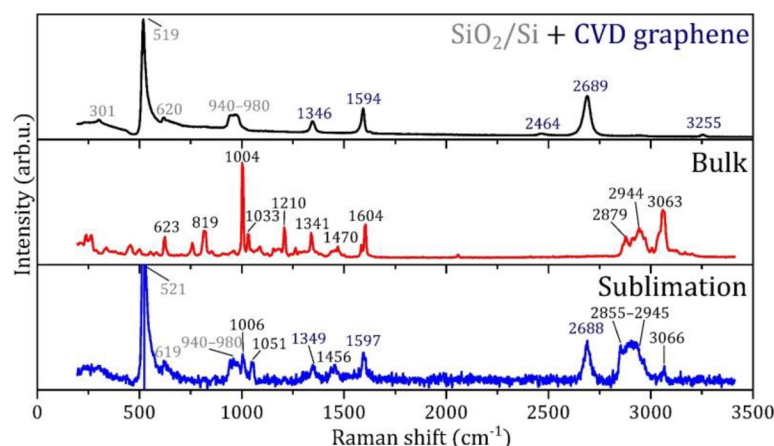
*Figure 7: Comparison of Raman spectra, from top to bottom, of the substrate: CVD graphene (Raman shift values marked in dark blue) on SiO2/Si (marked in grey), bulk **2a** and deposited **2a** by thermal sublimation (marked in black).*

XPS spectra show chemical composition for bulk and sublimated **2a** (**Figure 8**). Both survey spectra exhibited photoelectron peaks: Co 2p, N 1s, Cl 2p, C 1s, and O 1s; and Augers peaks: O_{KLL} and Co_{LMM}. In the case of bulk spectrum, Sn 3d peak was observed. This contamination likely originated from a synthetic process of the ligand trenb. The detailed spectra of the selected peaks unveiled specific chemical composition. Co 2p peak of the bulk **2a** exhibited two main components Co $2p_{3/2}$ and Co $2p_{1/2}$ and shake-up satellites, which are common with paramagnetic states[99]. The oxidation state depends on spin-orbit splitting of the main components Co $2p_{3/2}$ and Co $2p_{1/2}$, and with $\Delta = 15.5$ eV, it corresponds to Co(II) in the high-spin state[100]. In the case of the sublimated sample, the Co 2p signal is weak. However, it was possible to observe and fit the peak Co $2p_{3/2}$ and the satellite, which was shifted with respect to the peak of the bulk (0.9 eV and 1.4 eV to higher binding energy, respectively).

In the case of N 1s of the bulk, the peak included five components. The main component corresponds to the amine at 399.9 eV, and two smaller peaks at 398.5 eV and 402.8 eV were attributed to the azido group[101,102]. The smallest peak at 406.3 eV may be attributed to chemisorbed nitrogen[103]. The origin of the fifth peak at 397.1 eV may correspond to unreacted azide[104]. In the case of the sublimated sample, the main component and chemisorbed nitrogen were shifted by 0.5 eV and 0.8 eV to higher binding energy, and a new peak appears at 401.9 eV. Components characteristic of the azido ligand are no longer present.

Considering the changes in the ratio of the peaks in the Raman spectrum and especially in the XPS spectrum of nitrogen, where we did not observe peaks of the azido group and a new peak appears, it indicated possible sample decomposition during the sublimation.
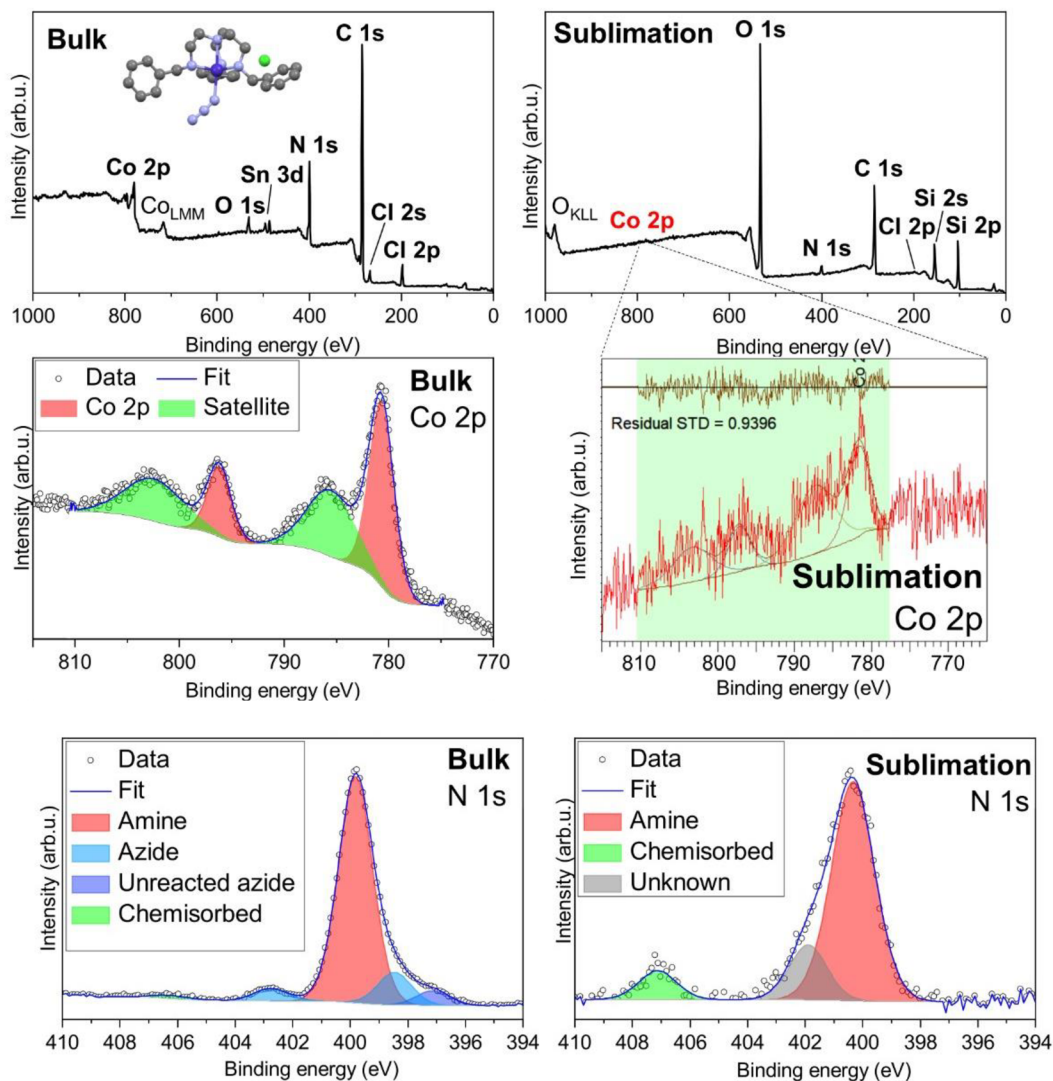
*Figure 8: Comparison of XPS spectra of the bulk and sublimated **2a** on graphene.*

TGA performed on **2c** revealed abrupt weight loss at temperatures above 250 °C. The morphology of the sample after sublimation on surface was probed by AFM and SEM. This decomposition was corroborated by comparison of bulk and sublimated **2a** by Raman and XPS. Raman spectra of sublimated compound on surface did not show signature vibrational molecular peaks.

The deposition of **2b**, **2c**, **2d** and **2j** were performed and the hybrid materials were investigated by Raman and XPS resulting in even larger spectral changes than was observed for **2a**.

As a conclusion, it was found out that despite of having favorable molecular geometry the physical parameters of the presented trenb complexes were not suitable for wet or sublimation deposition techniques.

5.3   Mono and Polynuclear Complexes with H$_3$tipa Ligand

This chapter discusses synthesis of coordination compounds with the trigonal ligand H$_3$tipa. The suitability of this ligand for coordination of lanthanides was discussed in chapter 5.1, here will be coordination of this ligand to the Co(II) central atom discussed. The tetradentate nature of this ligand allows encapsulation of the Co(II) central atom with a possibility for additional coordination of the monodentate ligand resulting into coordination number 5. Moreover, the ligand H$_3$tipa can become a bridging ligand and induce formation of polynuclear coordination compounds. As will be discussed below, it was also revealed that in a basic solutions a Co(III) complex with the doubly or triply deprotonated H$_3$tipa ligan was formed and acted as metallo-ligand for coordinating the Co(II) atoms.

A series of the reactions with varying level of deprotonation of H$_3$tipa ligand and with varying monodentate ligands was designed and prepared yielding six coordination compounds. These complexes have been structurally, magnetically, and spectroscopically studied. The formulas of the studied complexes are following: [Co(H$_2$tipa)Cl]·CH$_3$OH (**3a**), [Co(H$_2$tipa)Cl]·CH$_3$OH (**3b**), [Co(H$_2$tipa)(NCS)]·H$_2$O (**3c**), (Et$_3$NH)[{Co(III)$_2$(Htipa)(tipa)(NCS)$_2$}Co(II)(NCS)$_2$] (**3d**), (Et$_3$NH)$_2$[{Co(III)$_2$(tipa)$_2$(NCS)$_2$}{Co(II)(NCS)$_2$}$_2$] (**3e**) and [{Co(III)$_2$(tipa)$_2$(H$_2$O)$_2$}{Co(II)Cl$_2$}$_2$]·H$_2$O·CH$_3$OH (**3f**).

5.3.1 Mononuclear Complexes with H$_3$tipa Ligand

Synthesis of **3a**, **3b** was done as followed: 1 mmol of CoCl$_2$·6H$_2$O/CoBr$_2$ was dissolved in 5 ml of MeOH and was added to the 5 ml MeOH solution of 1 mmol of H$_3$tipa and 1 mmol of Et$_3$N and stirred. Clear purple solution was filtered and crystalized by slow diffusion of diethyl ether into the mother liquor. Good quality purple crystals suitable for X-Ray diffraction studies were obtained this way.

Synthesis of **3c** was done by two different setups. As a first **3c** was prepared similarly to **3a** and **3b**. 1 mmol of CoCl$_2$·6H$_2$O in 5 ml of MeOH was mixed with solution of H$_3$tipa and Et$_3$N in 5 ml MeOH and 1 mmol of KNCS was added as a solid. However, this approach often led to occurrence of impurities such as **3a** or even **3d** and **3e**. To prepare pure **3c,** first **3a** or **3b** were prepared and isolated. Then they were used as a precursor and were dissolved in 5 ml of MeOH and 1 mmol of KNCS was added. The resulting solution produced good quality single crystal upon diffusion of diethyl ether into mother liquor.

Crystal structures:

The crystal structures were successfully determined for all the prepared coordination compounds of this series. **3a** and **3b** are isomorphous and crystalize in the $P2_1/c$ space group and both contain crystal solvate methanol. **3c** crystalizes in the $P2_1/n$ space group and contains one molecule of water as crystal solvate in its unit cell (**Figure 9**). The ligand H$_3$tipa is once deprotonated in the structures of **3a**, **3b** and **3c** and coordinates to the central Co(II) by one nitrogen and three oxygen donor atoms. The fifth position is occupied by the monodentate (pseudo)halogenido ligand Cl$^-$, Br$^-$ or NCS$^-$. The geometry of their coordination polyhedra is a little distorted trigonal bipyramid with following Addison parameters: τ(**3a**) =0.86, τ(**3b**) =0.84 and τ(**3c**) =0.79. The longest ML bonds are those with the halogenido ligands: d(Co-Cl) = 2.296(4) Å and d(Co-Br) = 2.453(1) Å. The Co–N bond with the isothiocyanido ligand is significantly shorter: d(Co-NCS) = 2.025(3) Å. The Co–N bonds with the nitrogen atoms of the H$_3$tipa ligand are very similar in the structure of all three compounds with the bond lengths ranging in the very narrow interval: d(Co-N) = 2.15 – 2.16 Å. This is similar also for the Co–O ML bonds with the protonated O-donor atoms (d(Co-OH) = 2.02 – 2.06 Å) or deprotonated O-donor atoms of the H$_2$tipa$^-$ ligand (d(Co-O) = 1.98 – 1.98 Å).

The crystal packing in **3a** and **3b** is organized by strong O-H···O hydrogen bonds (d(O-H···O) = 2.62-2.59 Å) that are formed between the protonated hydroxy groups of the H$_2$tipa ligand and solvate methanol molecules. Another type of the O–H···O hydrogen bond (d(O-H···O) = 2.66-2.69 Å) is formed between deprotonated hydroxy groups of the H$_2$tipa ligand and solvate methanol molecules (**Figure 9**). The crystal packing in **3c** is different since the O–H···O and O–H···S hydrogen bonds are present. The O-H···O hydrogen bonds (d(O-H···O) = 2.644(4) Å) are formed between the protonated hydroxy groups of the H$_2$tipa ligand and solvate water molecules. Another type of the O–H···O (d(O-H···O) = 2.737(3) Å) is formed between deprotonated hydroxy groups of the H$_2$tipa ligand and solvate water molecules. The O–H···S hydrogen bonds (d(O–H···S) = 3.368(3) Å) are formed between the sulfur atom from the isothiocyanido ligand and solvate water molecule (**Figure 9**). The presence of hydrogen bonds causes formation of supramolecular dimer of **3a**, **3b** and **3c**.
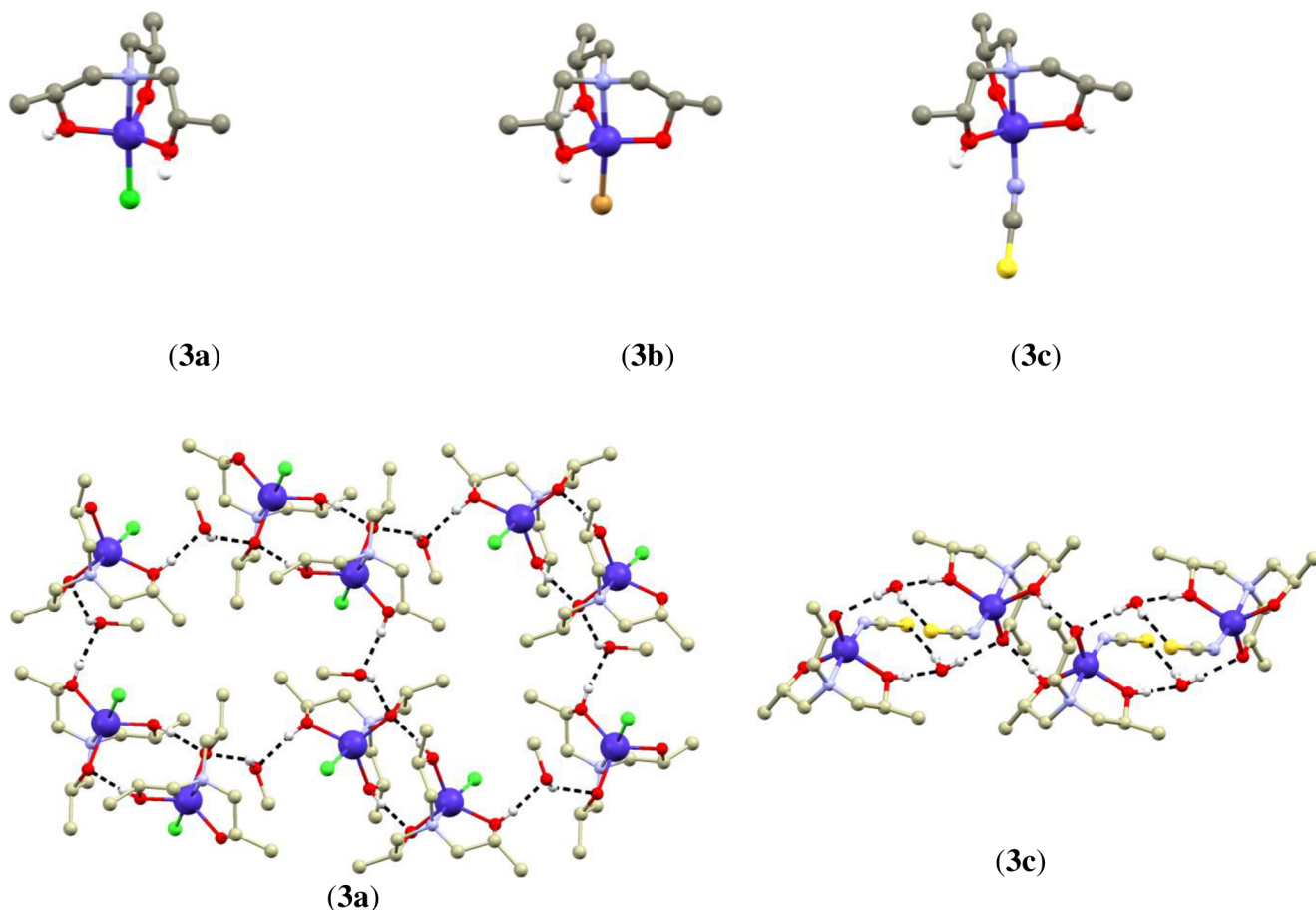
(3a)   (3b)   (3c)

(3a)

(3c)

*Figure 9: Depiction of crystal structures of **3a**, **3b** and **3c** and hydrogen bonds (blacked dashed lines) formed in crystal of **3a** and **3c**. Grey (C), light blue (N), purple (Co), green (Cl), yellow (S), red (O), white (H). The hydrogen atoms besides those involved in hydrogen bonding were ommited for clarity.*

Magnetic properties:

The maxima in the susceptibility plots of **3a-3c** visible at low temperatures (at ca. 7K) indicate a presence of non-negligible antiferromagnetic interactions in these compounds. Since these complexes are mononuclear the magnetic exchange pathways could be ascribed to the shortest non-covalent interactions assembling the $[Co(H_2tipa)X]$ molecules (X = Cl⁻, Br⁻, NCS⁻) into the supramolecular dimers via strong O−H···O hydrogen bonding (*vide supra*). Therefore, the magnetic data were analyzed by spin Hamiltonian for dimer with the exchange coupling, anisotropy and Zeeman terms:

$$\hat{H} = -J(\vec{S}_1 \cdot \vec{S}_2) + \sum_{i=1}^{2} D_i(\hat{S}_{z,i}{}^2 - \hat{S}_i{}^2/3) + E_i(\hat{S}_{x,i}{}^2 - \hat{S}_{y,i}{}^2) + \mu_B B g_i \hat{S}_{a,i} \qquad (1)$$

The magnetic data were depicted as temperature dependence of μ_{eff}/μ_B and field dependence of molar magnetization in Figure 49.

μ_{eff}/μ_B of **3a** and **3c** have similar at 300 K (5.42 and 5.22) and it decreases with temperature. The μ_{eff}/μ_B decreases at lower temperatures suggesting presence of ZFS and antiferromagnetic exchange coupling provided by strong hydrogen bonds. The temperature data follow similar pattern for all three compounds (**Table 4**).

The ZFS parameters and exchange interaction J are shown in **Table 4**. The magnetic anisotropy of **3a** and **3b** is small and axial and for **3c** is relatively big, all three compounds have large rhombicity.

Table 4: Summary of ZFS parameters and exchange interaction from fitting the magnetic data for positive and negative D.

	D	E/D	g_{iso}	J
3a	-6.61/6.59	0.33/0.29	2.03/2.03	-1.54/-1.60
3b	-8.87/8.70	0.33/0.33	2.17/2.17	-1.55/-1.54
3c	-14.37/14.27	0.33/0.33	2.13/2.13	-1.65/-1.66

Theoretical calculations:

*Table 5: Comparison of CASSCF calculations for **3a**, **3b** and **3c**.*

	D	E/D	g_{iso}
3a_1	-7.24	0.21	2.23
3a_2	-7.54	0.13	2.22
3a_3	-7.75	0.17	2.23
3b_1	-8.85	0.27	2.22
3b_2	-8.93	0.12	2.22
3b_3	-8.73	0.07	2.22
3c_1	-9.97	0.25	2.22
3c_2	-9.34	0.18	2.22
3c_3	-9.94	0.24	2.22

The CASSCF/NEVPT2 calculations were performed for **3a-3c** on three structural models (extracted from the corresponding crystal structures). The ZFS parameters were calculated for the following structural fragments:

1) supramolecular dimers {[Co(H$_2$tipa)X]···[Zn(H$_2$tipa)X]}, in which one of the Co(II) atoms was substituted by diamagnetic Zn(II) (**3a_1**, **3b_1** and **3c_1**).

2) monomers in the presence of the crystal solvates (methanol in **3a_2**, **3b_2**, H_2O in **3c_2**)
3) monomers (**3a_3**, **3b_3**, **3c_3**).

It was found that the choice of the structural fragment did not influence calculated values of the *D* parameter much, but rhombicity changed significantly (**Table 5**). The axial magnetic anisotropy is a relatively small but axial for **3a** and the |*D*| value is slightly growing for **3b** and **3c** respectively. This is in good agreement with the experimental values obtained by magnetometry (**Table 4**). The rhombicity was calculated largest for the dimeric fragments and therefore the better agreement with the magnetic measurements was achieved for calculations with the highest computational costs, especially in the case of **3a_1** and **3b_1**, whereas calculated rhombicity of **3c_1** and **3c_3** is comparable. The CASSCF/NEVPT2 calculations were also used to predict the ligand field parameters (AI-LFT procedure, **Figure 10**).

The magnetic anisotropy of **3a-3c** can be explained on basis of the calculated electronic structure. First, the splitting of the ^4F atomic term to ligand field terms (LFTs) resulted in first excited LFT being energetically separated from the ground state for about 4000 cm^{-1} (**Figure 10**). Therefore, the second-order spin orbital coupling can be expected to induce magnetic anisotropy. The splitting of the d-orbitals corresponds well with expectations for the trigonal bipyramidal geometry with the degenerate pairs of d_{yz}, d_{xz} and d_{xy}, $d_{x^2-y^2}$ orbitals (lowest in the energy), and d_{z^2} having the highest energy. Orbitals d_{yz} and d_{xz} are both occupied by two electrons, d_{xy}, $d_{x^2-y^2}$ and d_{z^2} are occupied with one electron each (**Figure 10**).
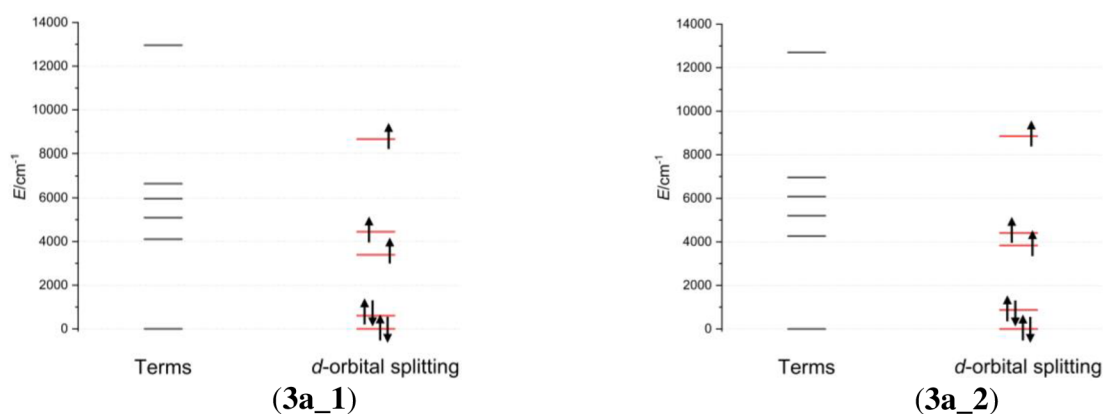

(**3a_1**)   (**3a_2**)

Figure 3: Graphical representation of the ligand field terms terms and d-orbital energy levels as calculated by CASSCF/NEVPT2 for complexes 3a_1 and 3a_2.

The magnetic exchange interaction in **3a-3c** was also studied theoretically by means of the Broken-Symmetry DFT (BS-DFT) which calculates energies of the selected polynuclear

fragments either with spins oriented parallelly (high-spin state, HS) and anti-parallelly (broken-symmetry state, BS). From the energy difference the isotropic exchange coupling constant is calculated using according to formulas established by L. Noodleman et al.[105,106], A. Bencini et al.[107] and Yamaguchi et al.[108] The BS-DFT calculations were performed at B3LYP/def2-TZVP level of the theory on the fragments selected from the crystal structures of **3a-3c**. The obtained results confirmed the assumption about dominant exchange pathway through the O–H···O hydrogen bonding within the supramolecular dimer. The spin density is localized dominantly on the metal centers; however, its part is distributed also on the oxygen atoms involved in the hydrogen bonding (**Figure 11**). The calculated exchange coupling constants are very similar for all three complexes and agrees rather well with the *J*-values determined from experimental data: J/cm^{-1} = −1.6 (**3a**), −1.6 (**3b**), −1.9 (**3c**).
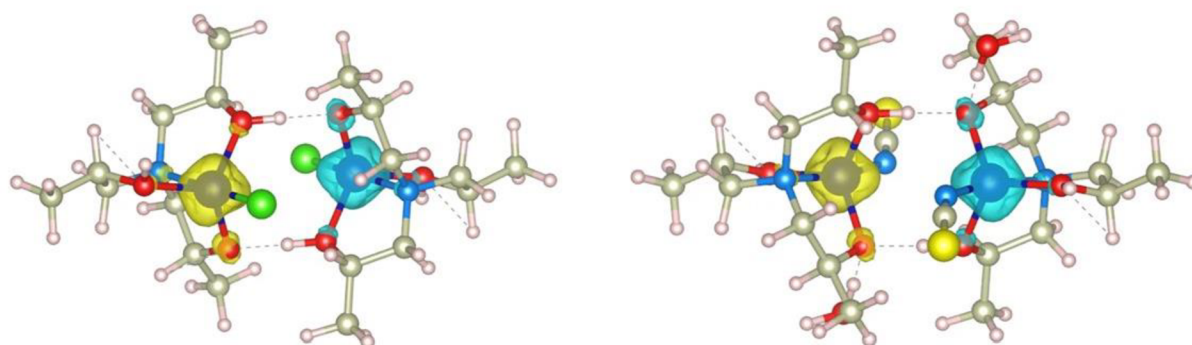

*Figure 4: Graphical representation of the calculated spin densities distribution for the broken-symmetry states of **3a** (left) and **3c** (right). Positive and negative spin densities are represented by yellow and blue surfaces, respectively. The isodensity surfaces are plotted with the cutoff values of 0.02ea$_0^{-3}$*

5.3.2 Tri- and Tetranuclear SMMs with H$_3$tipa Ligand
Synthesis:

Used stoichiometric ratios of reactants for preparation of **3d**, **3e** and **3f** did not correspond to the stoichiometry of the complexes. First, an extensive screening of the reactant ratios combined with titration investigation to investigate the influence of basis/KNCS concentrations (starting with stoichiometric ratios of 1:0 **3a**: KNCS up to 1:20 with varying combinations) on formation of **3d** and **3e** was performed. Based on the results of titration experiments it was revealed that, despite a weak basic nature of NCS⁻, it was not sufficient to treat solutions containing Co^{2+} ions and H$_3$tipa molecules only by KNCS to achieve both oxidation of cobalt ions and deprotonation of the H$_3$tipa ligand. Using UV-VIS spectrometry it was determined that for successful preparation is necessary combination of Et$_3$N and KNCS,

while using solely KNCS led the most probably to a formation of the $[Co(NCS)_4]^{2-}$ anions in titrated solutions[109] (**Figure 12**).
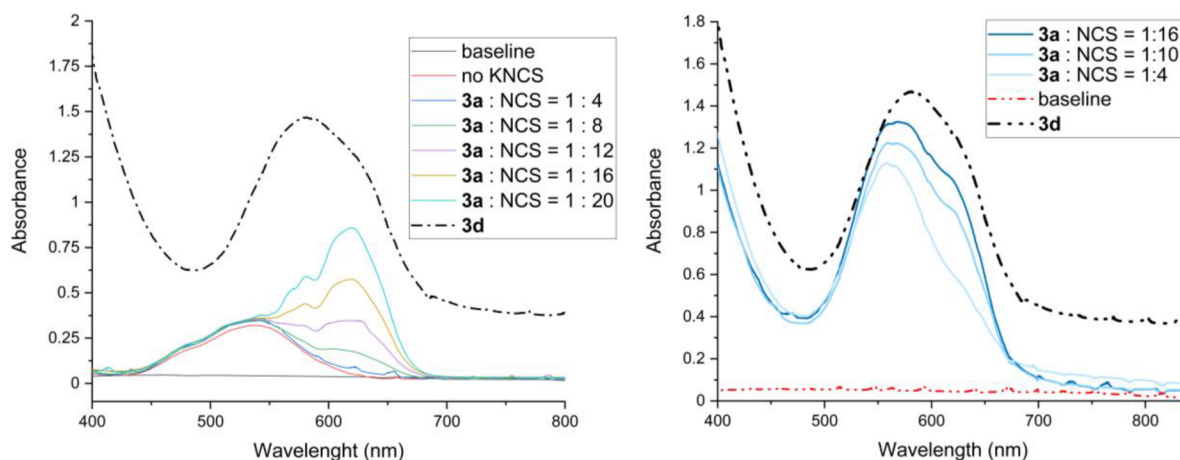

Figure 5: UV/VIS spectra of titration investigation of polynuclear H₃tipa complexes. Left – titration without base. Right – titration with base.

Pure batch of **3d** was prepared by reaction of $CoCl_2 \cdot 6H_2O$, H₃tipa, KNCS and Et₃N in molar ratios 1:2:4:4 in methanol (**Figure 13**). The solution was heated and stirred for 1 hour and filtered through the paper filter. Upon crystallization by slow diffusion of diethylether into mother liquor, the good quality crystals were acquired. If the reaction was heated for too long and the volume of methanolic solution was significantly reduced (more than one fourth of the volume) a crystallization of **3a** occurred.

Similar reaction setup was used to prepare pure **3e** where the reaction ratios were 2:1:3:3 (**Figure 13**).

A bottom-up synthesis for **3d** and **3e** was also tested by reacting **3c** with $Co(NCS)_2$ in different ratios (1:1 for **3d** and 1:2 for **3e**) in basic methanolic solutions (Et₃N). Resulting solutions were crystallized by slow diffusion of diethylether forming a blue microcrystalline slurry which was recrystallized in acetone and again crystallized by slow diffusion of diethylether. This way the crystals of **3d** and **3e** were obtained but in the minimal yield (5%).
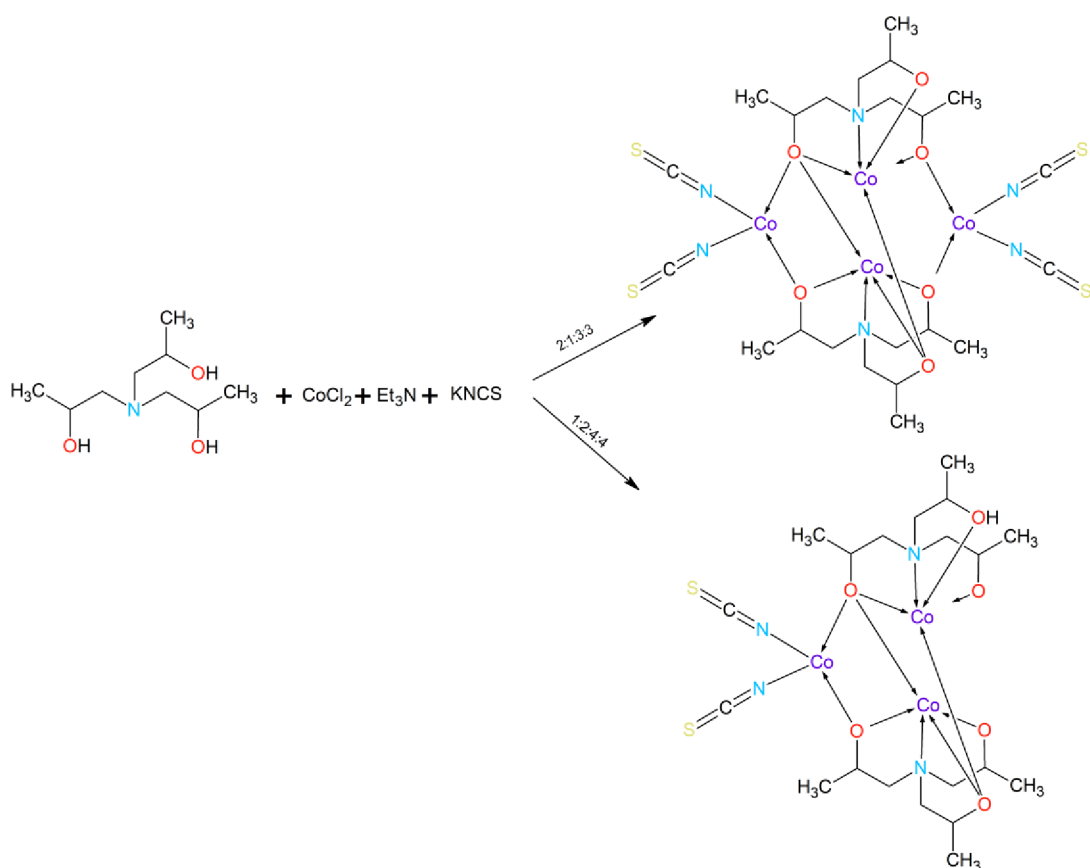
*Figure 6: Synthetic scheme of preparation of compounds **3d** and **3e**.*

3f was prepared only by reaction in microwave reactor. 1 mmol of CoCl$_2$·6H$_2$O, 1 mmol of H$_3$tipa and 1 mmol of Et$_3$N in 5 ml of iPrOH were mixed and placed in the Anton Paar reaction vessel and heated up at 120 °C for 10 minutes. Resulting blue solution was filtered through the paper filter and crystallized by slow diffusion of diethyl ether producing good quality crystals (**Figure 14**).

*Figure 7: Synthetic scheme for preparation of compound **3f**.*

Compound **3d** crystalizes in the monoclinic space group $P2_1/c$. This trinuclear complex molecule is not electroneutral and its charge is balanced by the Et_3NH^+ cation. The complex anion $[\{Co_2(Htipa)(tipa)(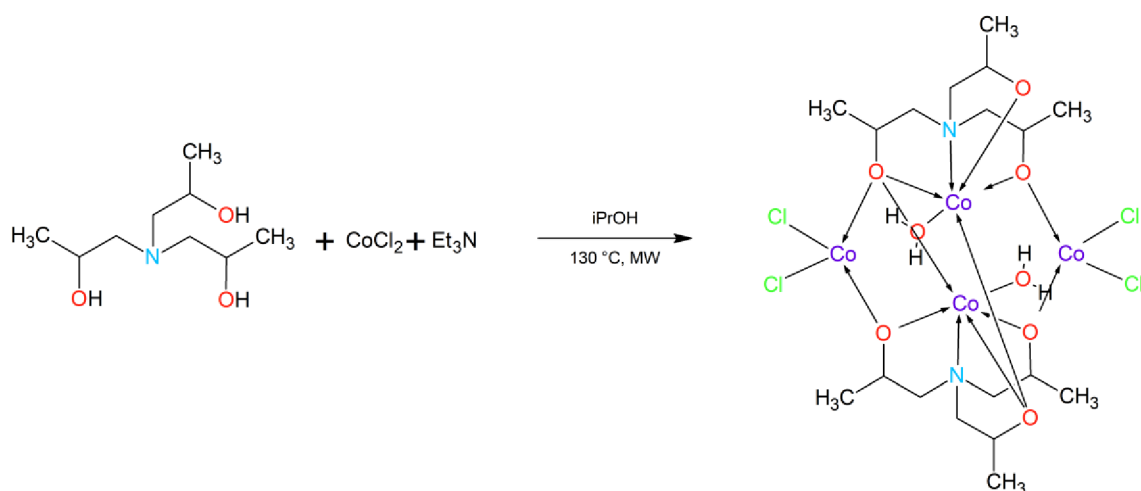NCS)_2\}\{Co(NCS)_2\}]^-$ is composed of two hexacoordinate Co(III) subunits $\{Co_2(Htipa)(tipa)(NCS)_2\}^-$, which are bridged by the deprotonated μ-O atoms of two H_3tipa ligands. The sixth positions are occupied by the NCS^- ligands. These bonds are rather short d(Co–O) = 1.88-1.93 Å, d(Co–N) = 1.90-1.92 Å, which corresponds with their low spin state and oxidation number (III). The third Co center is tetracoordinated by two oxygen atoms from the Co(III) subunits and by two NCS^- ligands (**Figure 15**). The bond lengths are longer than for Co(III) suggesting the oxidation number (II): d(Co–O) = 1.99-2.00 Å, d(Co–N) = 1.97-1.99 Å. The oxygen atoms from the H_3tipa ligand are forming strong intramolecular hydrogen bonds d(O⋯O) = 2.434(3) Å. Another type of N–H⋯S hydrogen bonding is formed between the sulphur atom of one of the NCS^- ligands and amine group from the Et_3NH^+cation: d(N⋯S) = 3.304(6) Å.

The compound **3e** crystalizes in the monoclinic space group $P2_1/c$ and consist of two Et_3NH^+ cations balancing charge of the complex anion $[\{Co_2(tipa)_2(NCS)_2\}\{Co(NCS)_2\}_2]^{2-}$, which is centrosymmetric (**Figure 15**). The Co(III) atoms are coordinated in the same manner as in **4b** with one difference, both the H_3tipa ligands are fully deprotonated. The subunits $\{Co_2(tipa)_2(NCS)_2\}^{2-}$ work as bridging metallo-ligands and their central atoms adopt the low-spin state with rather short bond lengths d(Co-N) = 1.90-1.92 Å, d(Co-O) = 1.90-1.95 Å. They are coordinating two tetracoordinate subunits $\{Co(NCS)_2\}_2$ which are both coordinated by two oxygen atoms of the H_3tipa ligand and two nitrogen atoms from NCS^- monodentate ligands. The geometry of coordination polyhedron is distorted tetrahedral. The bond lengths are again longer for the Co(II) high spin centres d(Co-N) = 1.97-2.00 Å, d(Co-O) = 1.90-1.96 Å. The Et_3NH^+ cations form N–H⋯S hydrogen bonds with the NCS^- ligands d(N⋯S) = 3.283(4) Å.

The compound **3f** crystalizes in the monoclinic space group $P2_1/n$ and with two crystal solvate methanol and two water molecules per complex molecule and the structure is centrosymmetric (**Figure 15**). The structure of **3f** differs from **3d** and **3e** by absence of the cations balancing the charge as **3f** is electroneutral. The compound contains two subunits coordinated by the H_3tipa ligand in the same manner as it is for **3e** with all the hydroxy groups being deprotonated and with one important difference causing electroneutrality of the complex molecule - the sixth position is occupied by aqua ligand: $[\{Co_2(tipa)_2\}\{CoCl_2\}_2]$. The metal-

ligand bond lengths are: d(Co–O) = 1.87-1.96 Å, d(Co–N) = 1.92 Å. This confirms that the Co centers are in the low-spin state and in the oxidation state (III). The two tetracoordinated Co centers in the {CoCl$_2$}$_2$ moiety are coordinated by two oxygen atoms from the H$_3$tipa ligand and by two chlorido ligands. The geometry of coordination polyhedral is distorted tetrahedral with longer coordination bonds than were observed for Co(III) fragment: d(Co–O) = 1.95-1.96 Å, d(Co–Cl) = 2.28-2.29 Å. Thus, the Co centers are in the high-spin state and having oxidation number (II). The water crystal solvate molecules are forming the O–H···O hydrogen bonds with aqua ligand d(O···O) = 2.692(4) Å. Relatively strong O–H···Cl hydrogen bonds are also formed between crystal solvate and aqua ligand d(O···Cl) = 2.710(5) Å.

(3d)   (3e)   (3f)
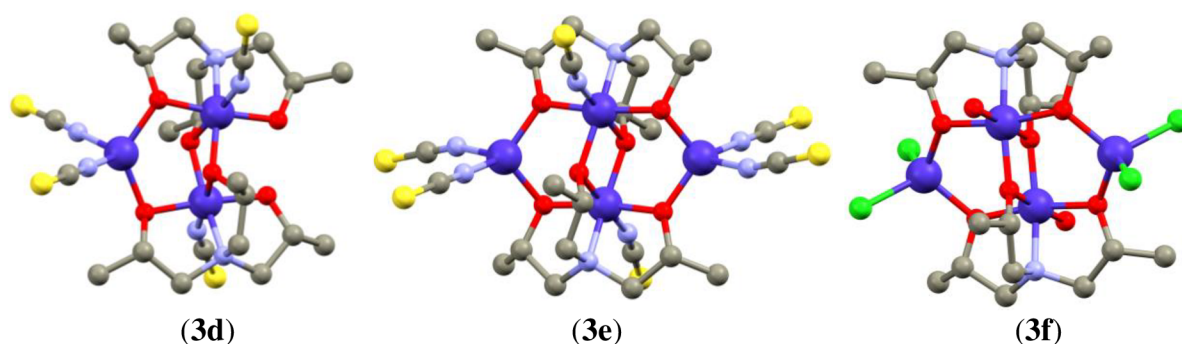
*Figure 8: Depiction of the complex molecules from the crystal structures of **3d**, **3e** and **3f**. Purple (Co), grey (C), red (O), light blue (N), green (Cl), yellow (S), hydrogen atoms were omitted for clarity.*

Magnetic properties:

3d, **3e** and **3f** contains Co(II)–Co(III) mixed-valence complex molecules containing with one (**3d**) or two (**3e**, **3f**) paramagnetic Co(II) centers. This composition difference indeed influences the magnetic response of the samples.

The effective magnetic moment of **3d** has value of 4.15 at 300 K, which is larger than spin only value (μ_{eff} = 3.87 μ_B for g = 2.0023 and S = 3/2) indicating spin-orbital contribution to the ground state. The μ_{eff}/μ_B value decreases very gradually with temperature and below 50 K, the decrease becomes more pronounced (3.2 at 2 K). With respect to the crystal structure of **3d** the observed decrease of μ_{eff} below 50 K can only be ascribed to the zero-field splitting (ZFS), and therefore, the magnetic data were analyzed using the ZFS spin Hamiltonian (**Equation 1**and **Table 6**). The fitting of magnetic data resulted in the following set of parameters: g = 2.14, D = -17.2 cm^{-1} a E/D = 0.02. Thus, the magnetic anisotropy in **3d** is relatively large, axial with a low rhombicity. This makes **3d** to be a good candidate for observation of slow-magnetic relaxation.

The μ_{eff}/μ_B value for **3e** is 6.0 at (μ_{eff} = 5.48 μ_B) 300 K and remains constant down to 50 K and on further cooling it drops to 2.8 at 2 K (**Table 6**). Such behavior indicates ZFS together with antiferromagnetic type of magnetic coupling between two Co(II) ions in **3e** separated on relatively short distance (5.76 Å). Therefore, besides the ZFS terms also the magnetic exchange coupling term was included into analysis of the magnetic data (**Equation 1**). The two sets of the fitted parameters sufficiently reconstructed the experimental data (one with $D{>}0$, second for $D{<}0$, **Table 6**). The exchange interaction between the Co(II) centers was fitted to be J = -0.59 cm^{-1} for $D{<}0$, or J = -0.83 cm^{-1} for $D{>}0$.

The μ_{eff}/μ_B value for **3f** is 5.5 (μ_{eff} = 5.48 μ_B) at 300 K and gradually decreases down to 5.2 at 50 K where a sudden drop occurs to 2.3 at 3 K (**Table 6**). Similarly, to **3e**, this indicates a presence of magnetic exchange interaction together with ZFS. Therefore, the spin Hamiltonian including the ZFS and exchange terms were used (**Equation 1 Table 6**). The exchange interaction between the Co(II) atoms was fitted to be J = -1.3 cm^{-1}.

Despite the rather similar Co(III) metallo-ligand and tetracoordinate nature of the Co(II) central atoms in both **3e** and **3f**, the magnitude of D differs significantly. Another puzzling thing is difference in magnitude of the exchange coupling constant J -obviously the exchange interaction is mediated through the shortest possible super-exchange pathway, which is in this case Co(II)–O–Co(III)–O–Co(II) pathway. This is shorter (7.67 Å) for **3e** which exhibits weaker exchange interaction than **3f** possessing longer pathway (7.75 Å).

*Table 6: ZFS parameters and exchange interaction J obtained from the magnetometry for **3d**, **3e** and **3f**.*

	D	E/D	g_{iso}	J
3d	-17.2	0.02	2.14	–
3e	-13.8/+12.9	0.00/0.33	2.19/2.19	-0.59/-0.83
3f	9.5	0.00	1.99	-1.3

For **3d** have been performed also dynamic magnetic measurements. Under the small static external field (B_{DC} = 0.1 T) appeared out-of-phase susceptibility signal as frequency dependent maxima which confirms presence of the slow relaxation of magnetization in **3d**. Argand diagrams and Arrhenius law plot were constructed (**Figure 17**). The best fit provided following values: τ_0 = 4.1(3.9)·10^{-9} s and U_{eff} = 35.0(3.1) K. The U_{eff} obtained from Arrhenius law is in very good agreement with a value calculated: U_{eff} = 34.4 K.
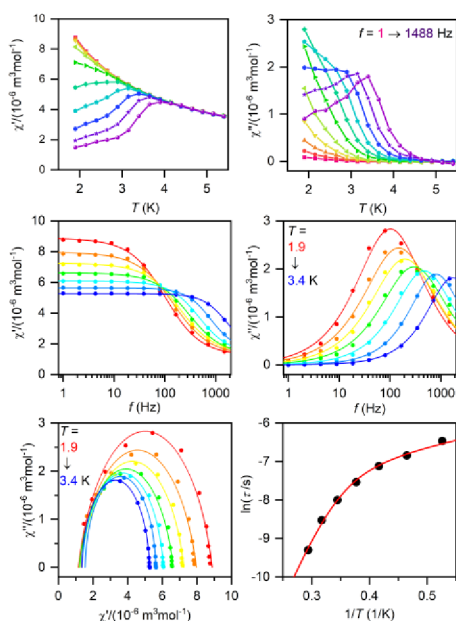
*Figure 9:The AC measurements of **3d**, temperature dependent data (top), frequency dependent data (middle), Argand diagram (left bottom) and Arrhenius diagram (right bottom).*

Theoretical calculations:

The analysis of magnetic data was supported by the CASSCF/NEVPT2 theoretical calculations, which were utilized to calculate all energy levels resulting from the $3d^7$ electronic configuration (**Figure 18**) with the ORCA 4.2 computational package[82]. The cation(s) (Et_3NH^+) were also involved in the calculations due to the fact that they form hydrogen bonds to the coordinated isothiocyanido ligands, and previously (and also for **3a-3c** in this thesis) it was found that such weak interaction can have significant impact on ZFS parameters[110,111].

*Table 7: Calculated ZFS parameters of **3d**, **3e** and **3f**.*

	D	E/D	g_x	g_y	g_z
3d	-15.2	0.21	2.26	2.39	2.18
3e	8.09	0.32	2.24	2.30	2.18
3f	-4.69	0.28	2.26	2.29	2.33

The CASSCF/NEVPT2 calculations were performed to theoretically predict the values of the ZFS and ligand field parameters (AI-LFT procedure). ZFS data collected from the calculations are compared in **Table 7**. The axial parameter of magnetic anisotropy is negative for **3d** and its value is in a relatively good agreement with the magnetometry results. The D parameter calculated for **3e** is positive and again, agreement with the result provided by magnetometry (**Table 6**) is quite good. The largest disagreement between theory and experiment was observed for **3f**, for which the best fit of magnetic data gave the positive D

value, however, the calculations provided significantly smaller $|D|$ and with negative sign. Calculations predicted large rhombicity for all the complexes **3d-3f**. The calculated d-orbital splitting is characteristic for tetracoordinated species and weak ligand field (weakest for **3f, Figure 18**). The separation of the first LF term is satisfactory (1100 for **3d**, 1000 for **3e** and 1159 for **3f**) allowing use of spin Hamiltonian and confirming expected second-order SOC contribution.
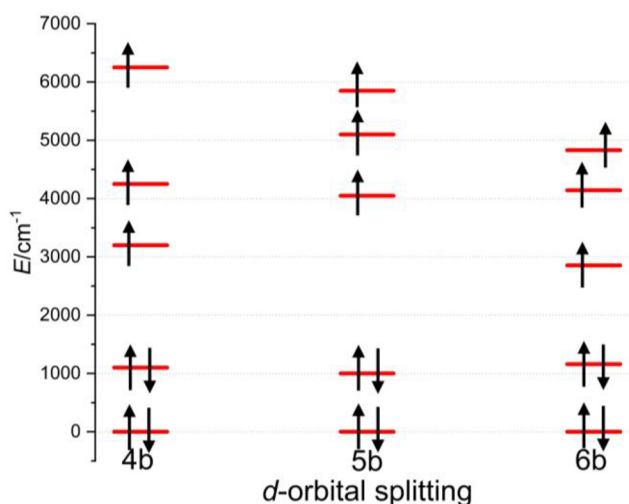
*Figure 10: Theoretical calculations of d-orbital energy levels for **3d**, **3e** and **3f**.*

The magnetic exchange interaction between the Co(II) atoms in **3e-3f** was also studied theoretically by BS-DFT calculations, which were performed at B3LYP/def2-TZVP level of the theory on the molecular structures selected from the crystal structures of **3e-3f**. The calculated spin density is localized dominantly on the metal centers; however, its part is distributed also on the oxygen atoms which supports hypothesis about the Co(II)–O–Co(III)–O–Co(II) magnetic exchange pathway (**Figure 19**). The calculated exchange coupling constants confirm antiferromagnetic coupling and agree rather well with the J-values determined from the experimental data: J/cm^{-1} = −0.4 (**3e**) and −2.2 (**3f**).
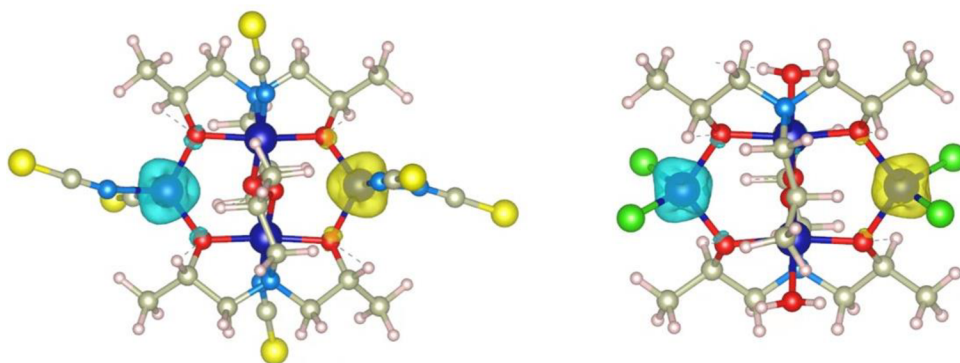
*Figure 11: Graphical representation of the calculated spin densities distribution for the broken-symmetry states of **3e** (left) and **3f** (right). Positive and negative spin densities are represented by yellow and blue surfaces, respectively. The isodensity surfaces are plotted with the cutoff values of $0.02 ea_0^{-3}$*

5.4 {M[Co(acac)₃]}ₙ Magnetic Chains

Organic molecule acetylacetone (acac) contains two possible O-donor atoms in its structure and it is rather sterically compact, potentially allowing high coordination numbers of the acetylacetonato complexes. Additionally, the preparation of the alkali metal salts of acac introduces new option which is interaction between the complex anion (in the case of Co(II) formation of $[Co(acac)_3]^-$ is expected) with the alkali metal cations, similarly as was described by Zadrozny et al. [35]. Thus, under appropriate conditions, the linear chain structure composed of alternating complex and alkali metal ion building blocks is expected to form and therefore, this type of coordination compounds are potential candidates for observation of the magnetic properties characteristic of SCM. For these reasons three acac salts have been prepared (namely Liacac, Naacac and Kacac) and coordinated to Co(II) affording following coordination compounds – Li[Co(acac)₃] (**4a**), Na[Co(acac)₃] (**4b**) K[Co(acac)₃] (**4c**) (**Figure 21**).

The structure of the studied acetylacetonate Co(II) complexes have been previously published in the literature [112–114] and remarkably, the Li salt has been investigated as precursor for preparation of non-aqueous redox flow cells with applications in batteries[115]. In this thesis the modified and simplified synthesis of the **4a**, **4b** and **4c** is reported: 4 mmol of NaOH/KOH/LiOH·H₂O was dissolved in 5 ml of MeOH and 4 mmol of acac was added and the mixture was stirred. 1 mmol of CoCl₂·6H₂O was added to the solution and it was stirred overnight. A purple powder was filtered through the paper filter and the mother liquor was left for isothermal crystallization. After 3-7 days purple needle shaped crystals suitable for single crystal diffraction formed.

Crystal structure:

As was mentioned above the crystal structures of the discussed compounds were previously published, here discussed as the crystal structures were obtained at low temperature in this thesis.

Compound **4a** crystalizes in the $R\overline{3}c$ space group. The Co–O bonds have all the same length: d(Co–O) = 2.052(2) Å. The threefold main axis parallel to the c-axis goes through the Co and Li atoms, whereas three two-fold axes each going through the middle carbon atom of the acac ligand are perpendicular to the threefold main axis. The two-fold axes are perpendicular to the main axis and together with the absence of horizontal and diagonal planes this gives D_3 symmetry of the complex subunit. The charge of the [Co(acac)$_3$]$^-$ is compensated by the Li$^+$ cation. The lengths of the interactions between the ligand's oxygen atoms and the Li$^+$ cation are all equal: d(Li$^+\cdots$O) = 2.135(5) Å. The chain-like structure of **4a** propagates along the c crystallographic axis with the angle Li–Co–Li being 180° (**Figure 20**). The distance between Co and Li$^+$ is d(Co-Li$^+$) = 2.738(4) Å and it is longer than in **4b,** but the distance between two in-chain neighbouring Co centres is shorter d(Co$\cdots$Co) = 5.471(4) Å (**Figure 21**).

Compound **4b** isostructural to **4a** crystalizes in the $R\overline{3}c$ space group. Three bidentate acac ligands are coordinating the Co center by two O-donor atoms each and all having the same length d(Co-O) = 2.069(3) Å. Again, the local symmetry of the complex part is D_3.

The charge of the [Co(acac)$_3$]$^-$ is compensated by the Na$^+$ cation. The oxygen atoms of ligand for interactions with the cation all of equal lengths d(Na$^+\cdots$O) = 2.346(1) Å as well as with the cation of the neighboring unit. The chain-like structure of **4b** propagates along the c crystallographic axis holding thus linear Na–Co–Na angle. The distance between Co and Na$^+$ is rather short: d(Na$^+\cdots$Co) = 2.975(2) Å and distance between two in-chain neighbouring Co centres is 5.951(2) Å. These interactions and their influence on forming a chain-like structure (**Figure 21**) is similar to that described by Zadrozny et al[35].

Compound **4c** differs from **4a** and **4b**. It crystalizes in the monoclinic space group Pna2$_1$. In the crystal structure there are several features like in **4a** and **4b**. The charge of the [Co(acac)$_3$]$^-$ is compensated by the K$^+$ cation. The Co centre is coordinated by oxygen atoms of the three acac ligands, however in **4c** their bond lengths are not equal, but varying within the narrow range: d(Co-O) = 2.06-2.09 Å. The K–O bonds lengths also differs with d(O-K$^+$) = 2.6-2.79 Å. The distance between the Co and K atoms is d(Co$\cdots$K$^+$) = 3.389(2) Å and it is longer than in **4b**, while the distance in between two in-chain Co centres is shorter d(Co-Co) = 6.611(2)

Å. The structure of **4c** does not propagate itself along the crystallographic *a*-axis in the linear manner and the Co–K–Co angle is 153.86(8)° (**Figure 20**), though, the structure is still chain-like (**Figure 21**).

(a)

(b)

*Figure 20: View along crystallographic c-axis for **4a** a) and along a-axis for **4c** b). Purple (Co), pink (Li), dark pink (K), grey (C), red (O), hydrogen atoms are omitted for clarity.*

(**4a**)

(**4b**)

(**4c**)
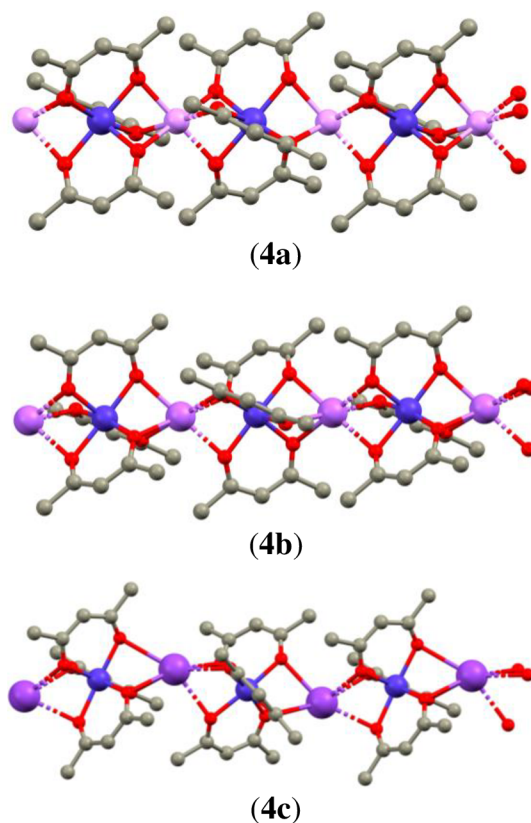
*Figure 21: Perspective view of a chain-like substructure of **4a**, **4b** and **4c**. Purple (Co), light pink (Li), pink (Na), dark pink (K), grey (C), red (O), hydrogen atoms are omitted for clarity.*

Theoretical calculations:

For the ideal D_3 symmetry, which was observed for **4a** and **4b,** the expected ground spin state (LF multiplet) for species with $S = 3/2$ is ^{4}E. Such ground term is orbitally degenerate and as such, it is a subject of the first order SOC producing huge and axial magnetic anisotropy[116,117]. The AILFT calculations revealed d-orbital splitting typical for trigonal prism, though this geometry does not correspond to that of coordination polyhedron in **4a** and **4b** as

41

can be confirmed by calculation of continuous measure indexes. The lowest energy was calculated for the orbital d_z^2 (two electrons), and two degenerate pairs d_{xy}, $d_{x^2-y^2}$ (three electrons) and d_{yz}, d_{xz} (two electrons) have higher energy. Thus, the total spin is $S = 3/2$ and the configuration is orbitally degenerate (**Figure 22**). The orbital splitting in **4c** is very similar to those calculated for **4a** and **4b**, however, the degeneracy of the d_{xy}, $d_{x^2-y^2}$ and d_{yz}, d_{xz} pairs is not perfect and they are separated by 67cm^{-1} (d_{xy}, $d_{x^2-y^2}$) and 333 cm^{-1}(d_{yz}, d_{xz}).
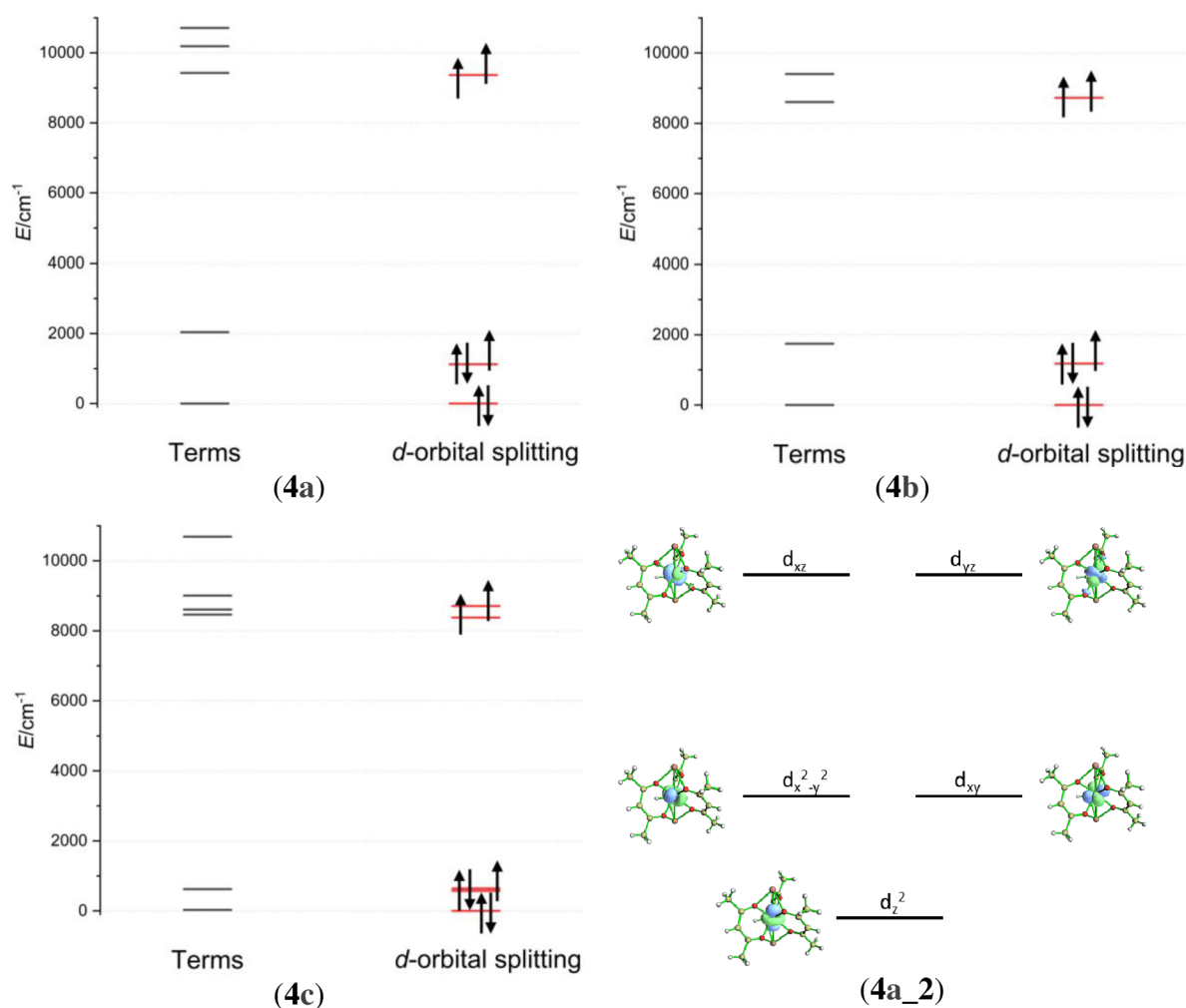
*Figure 22: Theoretical calculations of terms and d-orbital energy levels for **4a**, **4b** and **4c** and graphical depiction of the calculated orbitals by ab-initio ligand field theory in **4a** (**4a_2**).*

Due to the degeneration of the ground state (and non-applicability of spin Hamiltonian) it was not possible to calculate ZFS parameters for **4a** and **4b**. The calculated energy separation of the ground and first excited LF multiplets is 241 cm^{-1} (in **4a**) and 238 cm^{-1} (in **4b**). This indicates a very large magnetic anisotropy in these compounds. Calculation of the ZFS parameters for **4c** was successful, however, the calculated parameters must be taken with great

care because the first excited LF term adopt a rather low energy (30 cm^{-1}) and thus, spin Hamiltonian formalism is not applicable.

The BS-DFT calculations were used to determine possible magnetic interactions between the in-chain lining Co(II) atoms with the expected Co–M_a–Co exchange pathway (M_a = Li, Na, K). The calculations were performed at B3LYP/def2-TZVP level of the theory on the in-chain fragments as selected from the crystal structures of **4a-4c**. Remarkably, the calculations brought a rather surprising result. The magnetic exchange interaction was calculated to be negligible for **4a** ($J = 0.01$ cm^{-1}), which has the smallest in-chain separation between the Co atoms. The exchange interaction in **4b** was calculated to be weak and antiferromagnetic ($J = 2.50$ cm^{-1}). Again, weak and antiferromagnetic exchange interaction was calculated also for **4c** ($J = 1.74$ cm^{-1}). However, the energy of the ZFS splitting is in **4a-4c** that large, that splitting of the levels due to exchange interactions in **4b** and **4c** would be negligible.

Magnetic properties:

The μ_{eff}/μ_B of **4a** slowly decreases from 4.44 at 300K down to 3.99 at 70 K and decreases steeper further to 2.94 at 2.9 K.

The μ_{eff}/μ_B of **4b** has value of 4.79 at 300 K and it gradually decreases with temperature down to 3.68 at 3 K.

The μ_{eff}/μ_B of **4c** has value of 5.19 at 300 K and it gradually decreases with temperature down to 3.14 at 3 K.

In the previous chapter, we have shown that spin-Hamiltonian is not suitable for analysis of the magnetic data of **4a-c**. Nevertheless, the utilization of the L-S Hamiltonian based on Griffith and Figgis which describes the splitting of the $^4T_{1g}$ term originating from the ^4F atomic term in lower symmetries than O_h[118–121]. However, this approach did not bring any reasonable result. Therefore, to at least quantify apparent large magnetic anisotropy, the measured data were analyzed and fitted using Spin Hamiltonian using program POLYMAGNET[122]. The found ZFS parameters are shown in **Table 8**. The magnetic anisotropy is very large and for **4a** and **4c** is negative with small rhombicity. The magnetic anisotropy for **4b** is positive with maximal rhombicity.

*Table 8: ZFS parameters of **4a**, **4b** and **4b** obtained from Spin Hamiltonian fitting*

	D	E/D	g_{iso}

4a	-44.11	0.00	2.05
4b	75.02	0.33	2.43
4c	-80.23	0.00	2.05

6.   Conclusions

In first step this thesis focused on synthesis of trigonal organic ligands suitable for coordination of Dy(III) and Co(II) atoms. In the next step, it was planned to grow single crystals of prepared coordination compounds and study them structurally and magnetically. In the final step selected samples were supposed to be deposited on various substrates. The first and third step was complicated by issues of preparation of Dy(III) coordination compounds and thermal deposition of Co(II).

In section 5.1 is discussed preparation of a series of Mannich type ligands and attempts to prepare coordination compounds of them with Dy(III) as an central atom. A series of different Mannich ligands were prepared with great potential for synthesis of the Dy(III) coordination compounds with coordination number lower than usual 8 or 9. Despite many attempts made, the isolation of pure and crystalline products were unsuccessful.

Previously, many magnetically interesting Dy(III) coordination compounds with the H_3tea ligand were reported, so in this work H_3tea was replaced by more sterically demanding ligand H_3tipa. However, the preparation of wide series of structurally different complexes was not successful, while extensive screening of reaction conditions led only to preparation of dimeric complex **1a**. **1a** was structurally and magnetically studied. The magnetic data were analyzed using approach combining fitting of experimental data and ab initio calculations. This helped to reveal weak antiferromagnetic exchange interaction between the Dy(III) atoms of the dimer. From the theoretical calculations the value of spin-reversal barrier $U_{\mathrm{eff}} = 47.36$ cm^{-1} was obtained.

In section 5.2 it was possible to complete the series of coordination compounds with the trigonal ligand trenb reaching total amount of twelve coordination compounds. The series was extensively experimentally and computationally studied. The magnetic measurements revealed that studied complexes possess small or medium axial magnetic anisotropy ($|D| = 1.8 - 9.4$ cm^{-1}). Additionally, the four compounds from the series were studied by HFEPR mostly confirming the magnetization studies and the measurements were also complemented by theoretical CASSCF/NEVPT2 calculations. Repeated attempts for utilization of the members of this series for depositions showed that they are not suitable for wet depositions (low solubility) nor for thermal sublimation (high temperature of sublimation).

Section 5.3 describes series of the Co-based coordination compounds with the H_3tipa ligand. Six coordination compounds were prepared– three mononuclear, one trinuclear and two tetranuclear. The preparation of the tri- and tetranuclear complexes was complicated and required extensive screening of the reaction conditions supported by titration and by UV/VIS characterization. This series is magnetically interesting due to the formation of the magnetic exchange pathways involving the non-covalent interactions. In the case of the mononuclear complexes, the O–H···O hydrogen bonding contributed to formation of the supramolecular dimers. The BS-DFT calculations confirmed this exchange pathway to mediate weak antiferromagnetic interactions (J_{CALC} = -1.7 to -1.5 cm^{-1}), which is in the excellent agreement with the results obtained from fitting of the magnetic data (J_{exp} = -1.9 to -1.6 cm^{-1}). In the case of tetranuclear complexes, the magnetic exchange interaction is mediated between the peripheral Co(II) atoms via the O–Co(III)–O exchange pathway. Again, the BS-DFT calculations supported this hypothesis and the agreement between the calculated (J_{CALC} = -0.6 cm^{-1} for **3e** and -1.3 cm^{-1} for **3f**) and experimentally obtained exchange coupling constants (J_{exp} = -0.4 cm^{-1} for **3e** and -2.2 cm^{-1} for **3f**) is excellent. AC susceptibility measurements were measured and analyzed for trinuclear Co(III)$_2$-Co(II) complex and it was revealed that this compound behaves as field-induced SIM with U_{eff} = 34.4 K.

From the magnetic point of view, the most perspective group of coordination compounds studied in this thesis are **4a**, **4b** and **4c**, discussed in section 5.4. These compounds are composed of the chains with alternating triacetylacetonato-Co(II) complex molecules and alkali cations (**Figure 66**) forming 1D chains. Li and Na salts have degenerate ground states, which should give a rise to large axial magnetic anisotropy. There is weak (Na, K salts) or even negligible (Li salt) magnetic exchange interaction between the molecules via exchange pathways involving alkali cations. The magnetic analysis of this series is very complicated, and it is still ongoing. Nevertheless, the obtained magnetization data corresponds with huge magnetic anisotropy.

7. References

1. Buschow, K. H. J., de Boer, F. R. *Physics of Magnetism and Magnetic Materials*. vol. 59 (World Scientific, 2003).

2. Lis, T. Preparation, structure, and magnetic properties of a dodecanuclear mixed-valence manganese carboxylate. *Acta Crystallogr. Sect. B Struct. Crystallogr. Cryst. Chem.* **36**, 2042–2046 (1980).

3. Hl-, N. I. H. G. *et al.* [Mn12012(02CR)16(H20)4]. 1804–1816 (1993).

4. Bogani, L. & Wernsdorfer, W. Molecular spintronics using single-molecule magnets. *Nanosci. Technol. A Collect. Rev. from Nat. Journals* 194–204 (2009) doi:10.1142/9789814287005_0020.

5. Barra, A. L., Debrunner, P., Gatteschi, D., Schulz, C. E. & Sessoli, R. Superparamagnetic-like behavior in an octanuclear iron cluster. *Europhys. Lett.* **35**, 133–138 (1996).

6. Yang, E.-C. *et al.* Cobalt single-molecule magnet. *J. Appl. Phys.* **91**, 7382 (2002).

7. Ishikawa, N., Sugita, M., Ishikawa, T., Koshihara, S. Y. & Kaizu, Y. Lanthanide double-decker complexes functioning as magnets at the single-molecular level. *J. Am. Chem. Soc.* **125**, 8694–8695 (2003).

8. Frost, J. M., Harriman, K. L. M. & Murugesu, M. The rise of 3-d single-ion magnets in molecular magnetism: towards materials from molecules? *Chem. Sci.* **7**, 2470–2491 (2016).

9. Bogani, L. & Wernsdorfer, W. Molecular spintronics using single-molecule magnets. *Nat. Mater.* **7**, 179–186 (2008).

10. Sessoli, R., Gatteschi, D., Caneschi, A. & Novak, M. A. Magnetic bistability in a metal-ion cluster. *Nature* **365**, 141–143 (1993).

11. Spree, L. *et al.* Robust Single Molecule Magnet Monolayers on Graphene and Graphite with Magnetic Hysteresis up to 28 K. *Adv. Funct. Mater.* **31**, 1–7 (2021).

12. Boča, R. *Chémia koordinačných a organokovových zlúčenin*. (Nakladateľstvo STU, 2011).

13. Wernsdorfer, W. Classical and Quantum Magnetization Reversal Studied in Nanometer-Sized Particles and Clusters. in *Handbook of Advanced Magnetic Materials* 77–127 (Springer US). doi:10.1007/1-4020-7984-2_3.

14. Gatteschi, D., Sessoli, R. & Villain, J. *Molecular Nanomagnets*. (Oxford University Press, 2006). doi:10.1093/acprof:oso/9780198567530.001.0001.

15. Benelli, C. & Gatteschi, D. *Introduction to Molecular Magnetism*. (Wiley-VCH Verlag GmbH & Co. KGaA, 2015). doi:10.1002/9783527690541.

16. Herchel, Radovan; Tuček, J. ;Trávníček Z. *Střídavá susceptibilita a vysokoteplotní magnetická měření a jejich využití v chemii a fyzice*. (Palacký University, 2009).

17. Borah, A. & Murugavel, R. Magnetic relaxation in single-ion magnets formed by less-studied lanthanide ions Ce(III), Nd(III), Gd(III), Ho(III), Tm(II/III) and Yb(III). *Coord. Chem. Rev.* **453**, 214288 (2022).

18. Aronica, C. *et al.* A Nonanuclear Dysprosium(III)–Copper(II) Complex Exhibiting Single-Molecule Magnet Behavior with Very Slow Zero-Field Relaxation. *Angew. Chemie* **118**, 4775–4778 (2006).

19. Sokol, J. J., Hee, A. G. & Long, J. R. A cyano-bridged single-molecule magnet: Slow magnetic relaxation in a trigonal prismatic MnMo6(CN)18 cluster. *J. Am. Chem. Soc.* **124**, 7656–7657 (2002).

20. Nemec, I. *et al.* Magnetic anisotropy and field-induced slow relaxation of magnetization in tetracoordinate CoII compound [Co(CH3-im)2Cl2]. *Materials (Basel).* **10**, 1–14 (2017).

21. Goswami, S., Mondal, A. K. & Konar, S. Nanoscopic molecular magnets. *Inorg. Chem. Front.* **2**, 687–712 (2015).

22. Sessoli, R. *et al.* High-Spin Molecules: [Mn12O12(O2CR)16(H2O)4]. *J. Am. Chem. Soc.* **115**, 1804–1816 (1993).

23. Chandrasekhar, V., Pandian, B. M., Vittal, J. J. & Clérac, R. Synthesis, structure, and magnetism of heterobimetallic trinuclear complexes {[L2Co2Ln][X]} [Ln = Eu, X = Cl; Ln = Tb, Dy, Ho, X = NO3; LH3 = (S)P[N(Me)N=CH-C6H 3-2-OH-3-OMe]3]: A 3d-4f family of single-molecule magnets. *Inorg. Chem.* **48**, 1148–1157 (2009).

24. Chakraborty, A., Acharya, J. & Chandrasekhar, V. Ferrocene-Supported Compartmental Ligands for the Assembly of 3d/4f Complexes. *ACS Omega* (2020) doi:10.1021/acsomega.0c00654.

25. Karasawa, S., Zhou, G., Morikawa, H. & Koga, N. Magnetic Properties of Tetrakis[4-(α - diazobenzyl)-pyridine]bis(thiocyanato-N)cobalt(II) in Frozen Solution after Irradiation. Formation of a Single-Molecule Magnet in Frozen Solution. *J. Am. Chem. Soc.* **125**, 13676– 13677 (2003).

26. Freedman, D. E. *et al.* Slow magnetic relaxation in a high-spin iron(II) complex. *J. Am. Chem. Soc.* **132**, 1224–1225 (2010).

27. Colacio, E. *et al.* Family of Carboxylate- and Nitrate-diphenoxo Triply Bridged Dinuclear Ni. *Inorg. Chem.* **51**, 5857–5868 (2012).

28. Li, H. *et al.* Remarkable Ln III 3 Fe III 2 clusters with magnetocaloric effect and slow magnetic relaxation. *Dalt. Trans.* **44**, 468–471 (2015).

29. Papatriantafyllopoulou, C., Wernsdorfer, W., Abboud, K. A. & Christou, G. Mn 21 Dy Cluster with a Record Magnetization Reversal Barrier for a Mixed 3d/4f Single-Molecule Magnet. *Inorg. Chem.* **50**, 421–423 (2011).

30. Chandrasekhar, V., Pandian, B. M., Azhakar, R., Vittal, J. J. & Clérac, R. Linear trinuclear mixed-metal CoII-GdIII-Co II single-molecule magnet: [L2Co2Gd][NO 3]·2CHCl3 (LH3 = (S)P[N(Me)N=CH-C 6H3-2-OH-3-OMe]3). *Inorg. Chem.* **46**, 5140–5142 (2007).

31. Chandrasekhar, V. *et al.* Cyclo- and Carbophosphazene-Supported Ligands for the Assembly of Heterometallic (Cu 2+ /Ca 2+ , Cu 2+ /Dy 3+ , Cu 2+ /Tb 3+) Complexes: Synthesis, Structure, and Magnetism . *Inorg. Chem.* **51**, 2031–2038 (2012).

32. Chandrasekhar, V., Dey, A., Das, S., Rouzières, M. & Clérac, R. Syntheses, structures, and magnetic properties of a family of heterometallic heptanuclear [Cu5Ln2] (Ln = Y(III), Lu(III), Dy(III), Ho(III), Er(III), and Yb(III)) complexes: Observation of SMM behavior for the Dy(III) and Ho(III) analogues. *Inorg. Chem.* **52**, 2588–2598 (2013).

33. Chandrasekhar, V. *et al.* Trinuclear heterobimetallic Ni2Ln complexes [L 2Ni2Ln][ClO4] (Ln = La, Ce, Pr, Nd, Sm, Eu, Gd, Tb, Dy, Ho, and Er; LH3 = (S)P[N(Me)N=CH-C6H 3-2-OH-3-OMe]3): From simple paramagnetic complexes to single-molecule magnet behavior. *Inorg. Chem.* **47**, 4918–4929 (2008).

34. Zadrozny, J. M. & Long, J. R. Slow magnetic relaxation at zero field in the tetrahedral complex [Co(SPh) 4] 2-. *J. Am. Chem. Soc.* **133**, 20732–20734 (2011).

35. Zadrozny, J. M., Telser, J. & Long, J. R. Slow magnetic relaxation in the tetrahedral cobalt(II) complexes [Co(EPh)4]2- (EO, S, Se). *Polyhedron* **64**, 209–217 (2013).

36. Mossin, S. *et al.* A Mononuclear Fe(III) Single Molecule Magnet with a 3/2↔5/2 Spin Crossover. *J. Am. Chem. Soc.* **134**, 13651–13661 (2012).

37. Zadrozny, J. M. *et al.* Magnetic blocking in a linear iron(I) complex. *Nat. Chem.* **5**, 577–581 (2013).

38. Fataftah, M. S., Zadrozny, J. M., Rogers, D. M. & Freedman, D. E. A mononuclear transition metal single-molecule magnet in a nuclear spin-free ligand environment. *Inorg. Chem.* **53**, 10716–10721 (2014).

39. Varzatskii, O. A. *et al.* Chloride ion-aided self-assembly of pseudoclathrochelate metal tris-pyrazoloximates. *Inorg. Chem.* **53**, 3062–3071 (2014).

40. Novikov, V. V. *et al.* A Trigonal Prismatic Mononuclear Cobalt(II) Complex Showing Single-Molecule Magnet Behavior. *J. Am. Chem. Soc.* **137**, 9792–9795 (2015).

41. Carl, E., Demeshko, S., Meyer, F. & Stalke, D. Triimidosulfonates as Acute Bite-Angle Chelates: Slow Relaxation of the Magnetization in Zero Field and Hysteresis Loop of a CoII Complex. *Chem. - A Eur. J.* **21**, 10109–10115 (2015).

42. Shao, F. *et al.* Tuning the Ising-type anisotropy in trigonal bipyramidal Co(II) complexes. *Chem. Commun.* **51**, 16475–16478 (2015).

43. Rechkemmer, Y. *et al.* A four-coordinate cobalt(II) single-ion magnet with coercivity and a very high energy barrier. *Nat. Commun.* **7**, 1–8 (2016).

44. Sottini, S. *et al.* Magnetic Anisotropy of Tetrahedral CoII Single-Ion Magnets: Solid-State Effects. *Inorg. Chem.* **55**, 9537–9548 (2016).

45. Zhu, Y. Y. *et al.* Zero-field slow magnetic relaxation from single Co(ii) ion: A transition metal single-molecule magnet with high anisotropy barrier. *Chem. Sci.* **4**, 1802–1806 (2013).

46. Bradley, D. C., Ghotra, J. S. & Hart, F. A. Three-co-ordination in Lanthanide Chemistry : *J. Chem. Soc., Chem. Commun.* 349–350 (1972).

47. Zhang, P. *et al.* Equatorially coordinated lanthanide single ion magnets. *J. Am. Chem. Soc.* **136**, 4484–4487 (2014).

48. Hänninen, M. M. *et al.* Two C 3 -Symmetric Dy 3 III Complexes with Triple Di-μ-methoxo-μ-phenoxo Bridges, Magnetic Ground State, and Single-Molecule Magnetic Behavior. *Chem. - A Eur. J.* **20**, 8410–8420 (2014).

49. Mylonas-Margaritis, I. *et al.* Using the Singly Deprotonated Triethanolamine to Prepare Dinuclear Lanthanide(III) Complexes: Synthesis, Structural Characterization and Magnetic Studies. *Magnetochemistry* **3**, 5 (2017).

50. Koroteev, P. S. *et al.* Mononuclear and binuclear lanthanide acetates with chelating and bridging triethanolamine ligands. *Polyhedron* **154**, 54–64 (2018).

51. Li, X., Liu, Y., Chi, X., Zhu, G. & Gao, F. Synthesis, Structures, and Magnetic Properties of Zigzag Tetranuclear Lanthanide Complexes. *Zeitschrift für Anorg. und Allg. Chemie* **646**, 1292–1296 (2020).

52. Langley, S. K., Moubaraki, B., Forsyth, C. M., Gass, I. A. & Murray, K. S. Structure and magnetism of new lanthanide 6-wheel compounds utilizing triethanolamine as a stabilizing ligand. *Dalt. Trans.* **39**, 1705–1708 (2010).

53. Goura, J. *et al.* Heterometallic Zn 3 Ln 3 Ensembles Containing (μ 6 -CO 3) Ligand and Triangular Disposition of Ln 3+ ions: Analysis of Single-Molecule Toroic (SMT) and Single-Molecule Magnet (SMM) Behavior. *Chem. - A Eur. J.* **23**, 16621–16636 (2017).

54. Chen, Y. C. *et al.* Symmetry-Supported Magnetic Blocking at 20 K in Pentagonal Bipyramidal

Dy(III) Single-Ion Magnets. *J. Am. Chem. Soc.* **138**, 2829–2837 (2016).

55.   Takamatsu, S., Ishikawa, T., Koshihara, S. Y. & Ishikawa, N. Significant increase of the barrier energy for magnetization reversal of a single-4f-ionic single-molecule magnet by a longitudinal contraction of the coordination space. *Inorg. Chem.* **46**, 7250–7252 (2007).

56.   Goodwin, C. A. P., Ortu, F., Reta, D., Chilton, N. F. & Mills, D. P. Molecular magnetic hysteresis at 60 kelvin in dysprosocenium. *Nature* **548**, 439–442 (2017).

57.   Guo, F. S. *et al.* A Dysprosium Metallocene Single-Molecule Magnet Functioning at the Axial Limit. *Angew. Chemie - Int. Ed.* **56**, 11445–11449 (2017).

58.   Guo, F. S. *et al.* Magnetic hysteresis up to 80 kelvin in a dysprosium metallocene single-molecule magnet. *Science (80-.).* **362**, 1400–1403 (2018).

59.   Kyatskaya, S. *et al.* Anchoring of rare-earth-based single-molecule magnets on single-walled carbon nanotubes. *J. Am. Chem. Soc.* **131**, 15143–15151 (2009).

60.   Lopes, M. *et al.* Surface-enhanced raman signal for terbium single-molecule magnets grafted on graphene. *ACS Nano* **4**, 7531–7537 (2010).

61.   Zhu, X., Hale, A., Christou, G. & Hebard, A. F. Electronegative ligands enhance charge transfer to Mn12 single-molecule magnets deposited on graphene. *J. Appl. Phys.* **127**, (2020).

62.   Cimatti, I. *et al.* Vanadyl phthalocyanines on graphene/SiC(0001): Toward a hybrid architecture for molecular spin qubits. *Nanoscale Horizons* **4**, 1202–1210 (2019).

63.   Marocchi, S. *et al.* Relay-Like Exchange Mechanism through a Spin Radical between TbPc2 Molecules and Graphene/Ni(111) Substrates. *ACS Nano* **10**, 9353–9360 (2016).

64.   Mannini, M. *et al.* Quantum tunnelling of the magnetization in a monolayer of oriented single-molecule magnets. *Nature* **468**, 417–421 (2010).

65.   Wäckerlin, C. *et al.* Giant Hysteresis of Single-Molecule Magnets Adsorbed on a Nonmagnetic Insulator. *Adv. Mater.* **28**, 5195–5199 (2016).

66.   Margheriti, L. *et al.* X-Ray Detected Magnetic Hysteresis of Thermally Evaporated Terbium Double-Decker Oriented Films. *Adv. Mater.* **22**, 5488–5493 (2010).

67.   Stepanow, S. *et al.* Spin and Orbital Magnetic Moment Anisotropies of Monodispersed Bis(Phthalocyaninato)Terbium on a Copper Surface. *J. Am. Chem. Soc.* **132**, 11900–11901 (2010).

68.   Mannini, M. *et al.* X-ray magnetic circular dichroism picks out single-molecule magnets suitable for nanodevices. *Adv. Mater.* **21**, 167–171 (2009).

69.   Cervetti, C. *et al.* The classical and quantum dynamics of molecular spins on graphene. *Nat. Mater.* **15**, 164–168 (2016).

70.   Addison, A. W., Rao, T. N., Reedijk, J., Rijn, J. van & Verschoor, G. C. Synthesis, Structure, and Spectroscopic Properties of Copper(II) Compounds containing Nitrogen-Sulphur Donor Ligands. *J. Chem. Soc. Dalt. Trans* **7**, 1349–1356 (1984).

71.   M. Llunell, D. Casanova, J. Ciera, P. Alemany, S. A. SHAPE, Version 2.1. (2013).

72.   Hrubý, J. High Frequency Electron Spin Resonance Spectroscopy. *PhD thesis* (Brno University of Technology, 2021).

73.   Hrubý, J. *et al.* Deposition of Tetracoordinate Co(II) Complex with Chalcone Ligands on Graphene. *Molecules* **25**, 1–17 (2020).

74.   Hrubý, J. *et al.* A graphene-based hybrid material with quantum bits prepared by the double Langmuir–Schaefer method. *RSC Adv.* **9**, 24066–24073 (2019).

75. Marie, L. S. *et al.* Nanostructured graphene for nanoscale electron paramagnetic resonance spectroscopy. *J. Phys. Mater.* **3**, 014013 (2020).

76. Sojka, A. *et al.* Sample Holders for Sub-THz Electron Spin Resonance Spectroscopy. *IEEE Trans. Instrum. Meas.* **71**, 1–12 (2022).

77. Stoll, S. & Schweiger, A. EasySpin, a comprehensive software package for spectral simulation and analysis in EPR. *J. Magn. Reson.* **178**, 42–55 (2006).

78. Ungur, L., Van den Heuvel, W. & Chibotaru, L. F. Ab initio investigation of the non-collinear magnetic structure and the lowest magnetic excitations in dysprosium triangles. *New J. Chem.* **33**, 1224 (2009).

79. Chibotaru, L. F., Ungur, L. & Soncini, A. The Origin of Nonmagnetic Kramers Doublets in the Ground State of Dysprosium Triangles: Evidence for a Toroidal Magnetic Moment. *Angew. Chemie Int. Ed.* **47**, 4126–4129 (2008).

80. Chibotaru, L. F. *et al.* Structure, Magnetism, and Theoretical Study of a Mixed-Valence Co II 3 Co III 4 Heptanuclear Wheel: Lack of SMM Behavior despite Negative Magnetic Anisotropy. *J. Am. Chem. Soc.* **130**, 12445–12455 (2008).

81. Neese, F., Wennmohs, F., Hansen, A. & Becker, U. Efficient, approximate and parallel Hartree-Fock and hybrid DFT calculations. A 'chain-of-spheres' algorithm for the Hartree-Fock exchange. *Chem. Phys.* **356**, 98–109 (2009).

82. Neese, F. Software update: the ORCA program system, version 4.0. *Wiley Interdiscip. Rev. Comput. Mol. Sci.* **8**, 1–6 (2018).

83. Anatasov, M.; Ganyushin, D.;Sivalingam, K. and Neese, F. *Molecular Electronic Structures of Transition Metal Complexes II*. vol. 143 (Springer Berlin Heidelberg, 2012).

84. Fairley, N. *et al.* Systematic and collaborative approach to problem solving using X-ray photoelectron spectroscopy. *Appl. Surf. Sci. Adv.* **5**, 100112 (2021).

85. Bazarnik, M., Brede, J., Decker, R. & Wiesendanger, R. Tailoring molecular self-assembly of magnetic phthalocyanine molecules on fe- and co-intercalated graphene. *ACS Nano* **7**, 11341–11349 (2013).

86. Danieli, C. *et al.* A novel class of tetrairon(III) single-molecule magnets with graphene-binding groups. *Polyhedron* **28**, 2029–2035 (2009).

87. Lisi, S. *et al.* Graphene-induced magnetic anisotropy of a two-dimensional iron phthalocyanine network. *J. Phys. Chem. Lett.* **6**, 1690–1695 (2015).

88. Jiang, H., Xie, Y. S., Zhou, Z. Y., Xu, X. L. & Liu, Q. L. Syntheses, structures and characterization of cobalt(II) and cobalt(III) complexes with N-benzylated polyamines and a terminal azido ligand. *J. Coord. Chem.* **56**, 825–832 (2003).

89. Xie, Y. S. *et al.* Syntheses and characterization of copper(II) and cobalt(II) complexes with tris[2-(benzylamino)ethyl]amine. *Collect. Czechoslov. Chem. Commun.* **67**, 1647–1657 (2002).

90. Havlíček, L. Magnetické vlastnosti a struktura pentakoordinovaných sloučenin Co(II) s tri- a tetradentátními ligandy odvozenými od alifatických triaminů. *Univerzita Palackého v Olomouci* (2018).

91. Mannini, M. *et al.* Magnetic memory of a single-molecule quantum magnet wired to a gold surface. *Nat. Mater.* **8**, 194–197 (2009).

92. Cornia, A. *et al.* Direct observation of single-molecule magnets organized on gold surfaces. *Angew. Chemie - Int. Ed.* **42**, 1645–1648 (2003).

93. Holmberg, R. J. *et al.* Hybrid nanomaterials: Anchoring magnetic molecules on naked gold

nanocrystals. *Inorg. Chem.* **52**, 14411–14418 (2013).

94. Cornia, A., Mannini, M., Sainctavit, P. & Sessoli, R. Chemical strategies and characterization tools for the organization of single molecule magnets on surfaces. *Chem. Soc. Rev.* **40**, 3076–3091 (2011).

95. Desiraju, G. & Steiner, T. *The Weak Hydrogen Bond*. (Oxford University Press, 2001). doi:10.1093/acprof:oso/9780198509707.001.0001.

96. Gomez-Coca, S., Cremades, E., Aliaga-Alcalde, N. & Ruiz, E. Mononuclear Single-Molecule Magnets: Tailoring the Magnetic Anisotropy of First-Row Transition-Metal Complexes. *J. Am. Chem. Soc.* **135**, 7010–7018 (2013).

97. Mazilu, M., De Luca, A. C., Riches, A., Herrington, C. S. & Dholakia, K. Optimal algorithm for fluorescence suppression of modulated Raman spectroscopy. *Opt. Express* **18**, 11382 (2010).

98. Larkin, P. *Infrared and Raman Spectroscopy*. (Elsevier, 2011).

99. J. F. Moulder, W. F. Stickle, P. E. S. and K. D. B. *Handbook of X-Ray Photoelectron Spectroscopy*. (J. F. Moulder, W. F. Stickle, P. E. Sobol and K. D. Bomben, Eden Prairie, Minnesota: Physical Electronics Division, Perkin-Elmer Corporation, 1992).

100. Poneti, G. *et al.* Magnetic and Spectroscopic Investigation of Thermally and Optically Driven Valence Tautomerism in Thioether-Bridged Dinuclear Cobalt–Dioxolene Complexes. *Inorg. Chem.* **52**, 11798–11805 (2013).

101. Solomon, E. I., Basumallick, L., Chen, P. & Kennepohl, P. Variable energy photoelectron spectroscopy: electronic structure and electronic relaxation. *Coord. Chem. Rev.* **249**, 229–253 (2005).

102. Lange, S. C., van Andel, E., Smulders, M. M. J. & Zuilhof, H. Efficient and Tunable Three-Dimensional Functionalization of Fully Zwitterionic Antifouling Surface Coatings. *Langmuir* **32**, 10199–10205 (2016).

103. Zhan, H. J. *et al.* Microwave Irradiation Synthesized Cobalt-Loaded Nitrogen-Doped Active Carbon as an Efficient Catalyst for Selective Oxidation of Ethylbenzene. *IOP Conf. Ser. Mater. Sci. Eng.* **562**, 012004 (2019).

104. Goldmann, A. S. *et al.* Surface Modification of Poly(divinylbenzene) Microspheres via Thiol−Ene Chemistry and Alkyne−Azide Click Reactions. *Macromolecules* **42**, 3707–3714 (2009).

105. Noodleman, L. Valence bond description of antiferromagnetic coupling in transition metal dimers. *J. Chem. Phys.* **74**, 5737–5743 (1981).

106. Noodleman, L. & Davidson, E. R. Ligand spin polarization and antiferromagnetic coupling in transition metal dimers. *Chem. Phys.* **109**, 131–143 (1986).

107. Bencini, A. & Gatteschi, D. X.alpha.-SW calculations of the electronic structure and magnetic properties of weakly coupled transition-metal clusters. The [Cu2Cl6]2- dimers. *J. Am. Chem. Soc.* **108**, 5763–5771 (1986).

108. Yamaguchi, K., Takahara, Y. & Fueno, T. Ab-Initio Molecular Orbital Studies of Structure and Reactivity of Transition Metal-OXO Compounds. in *Applied Quantum Chemistry* 155–184 (Springer Netherlands, 1986). doi:10.1007/978-94-009-4746-7_11.

109. Osborne, S. J. *et al.* Thermochromism and switchable paramagnetism of cobalt(<scp>ii</scp>) in thiocyanate ionic liquids. *Dalt. Trans.* **44**, 11286–11289 (2015).

110. Zoufalý, P., Čižmár, E., Kuchár, J. & Herchel, R. The structural and magnetic properties of FeII and CoII complexes with 2-(furan-2-yl)-5-pyridin-2-yl-1,3,4-oxadiazole. *Molecules* **25**, 1–18

(2020).

111. Herchel, R., Zoufalý, P. & Nemec, I. The effect of the second coordination sphere on the magnetism of [Ln(NO 3) 3 (H 2 O) 3]·(18-crown-6) (Ln = Dy and Er). *RSC Adv.* **9**, 569–575 (2019).

112. Harrah, B. No Title. *Microscope* **13**, 295 (1962).

113. Wei, Z., Han, H., Filatov, A. S. & Dikarev, E. V. Changing the bridging connectivity pattern within a heterometallic assembly: design of single-source precursors with discrete molecular structures. *Chem. Sci.* **5**, 813–818 (2014).

114. Li, X., Musie, G. & Powell, D. R. Sodium tris(acetylacetonato-κ 2 O , O ')cobalt(II). *Acta Crystallogr. Sect. E Struct. Reports Online* **59**, m717–m718 (2003).

115. Shin, S. H., Yun, S. H. & Moon, S. H. A review of current developments in non-aqueous redox flow batteries: Characterization of their membranes for design perspective. *RSC Adv.* **3**, 9095–9116 (2013).

116. Matos, C. R. M. O. *et al.* Field-induced single-ion magnets exhibiting tri-axial anisotropy in a 1D Co(<scp>ii</scp>) coordination polymer with a rigid ligand 4,4'-(buta-1,3-diyne-1,4-diyl)dibenzoate. *Dalt. Trans.* **50**, 15003–15014 (2021).

117. Świtlicka, A. *et al.* Field-induced slow magnetic relaxation in pseudooctahedral cobalt(<scp>ii</scp>) complexes with positive axial and large rhombic anisotropy. *Dalt. Trans.* **48**, 1404–1417 (2019).

118. Nemec, I., Herchel, R. & Trávníček, Z. Two polymorphic Co(<scp>ii</scp>) field-induced single-ion magnets with enormous angular distortion from the ideal octahedron. *Dalt. Trans.* **47**, 1614–1623 (2018).

119. Zoufalý, P., Kliuikov, A., Čižmár, E., Císařová, I. & Herchel, R. Cis and Trans Isomers of Fe(II) and Co(II) Complexes with Oxadiazole Derivatives - Structural and Magnetic Properties. *Eur. J. Inorg. Chem.* **2021**, 1190–1199 (2021).

120. Drahoš, B., Šalitroš, I., Císařová, I. & Herchel, R. A multifunctional magnetic material based on a solid solution of Fe(<scp>ii</scp>)/Co(<scp>ii</scp>) complexes with a macrocyclic cyclam-based ligand. *Dalt. Trans.* **50**, 11147–11157 (2021).

121. Ghosh, S. *et al.* Reversible Spin-State Switching and Tuning of Nuclearity and Dimensionality via Nonlinear Pseudohalides in Cobalt(II) Complexes. *Inorg. Chem.* **59**, 17638–17649 (2020).

122. Boča, R. MIF with FIT Module. (2019).

8. Author Publications and Other Outputs

Publications

- 2022 – L. Havlíček, R. Herchel, I. Nemec, P. Neugebauer. Weak antiferromagnetic interaction in Cu(II) complex with semi-coordination exchange pathway, *Polyhedron*, 223, 2022
- 2022 – X. Zhang, J. Kastyl, M. C. Luna, L. Havlíček, M. Vondra, V. Brummer, K. Sukačová, S. Y. Teng, P. Neugebauer. Microalgae-derived nanoporous biochar for ammonia removal in sustainable wastewater treatment, *Journal of Environmental Chemical Engineering*, 10, 2022

Oral contribution

- 2018 – PETER Summer School, Brno, Czech Republic
- 2019 – 12th European School on Molecular Nanoscience and 7th Workshop on 2D Materials, Elche, Spain

Posters

- 2018 – ICN+T, Brno, Czech Republic
- 2018 – PETER Summer School, Brno, Czech Republic
- 2021 – ICMM 17th International Conference on Molecule Based Magnets, online

Supervision

- 2019 - CEITEC Student Talent supervision of Vojtěch Richard Krejsa (2nd place), Brno, Czech Republic

Grants

- 2018-2019 - VUT Specific research
- 2020-2021 - VUT Specific research - publication

Teaching activities

- September-December 2019 - Teaching Seminar of General chemistry (prof. Jiří Pinkas at MU, Brno, Czech Republic)
- September-December 2020 – Teaching Chemical Synthesis practicum (Dr. Slávka Janků at MU, Brno, Czech Republic)
- 2019 – one hour presentation in Diploma Seminar (prof. Jiří Pinkas at MU, Brno, Czech Republic)

Internships

- 2019 – one month in a group of prof. Song Gao, Beijing, China
- 2019 – two weeks in a group of prof. Nikodem Kuźnik, Gliwice, Poland
- 2021 – one week in a laboratory of Assoc. prof. Ivan Šalitroš, Bratislava, Slovakia
- 2021 – one month in a group of prof. Paola Barbara, Washington DC, USA

Voluntary activities

- 2018, 2019 – Researcher's Night, CEITEC BUT, Brno, Czech Republic
- 2019 – 2021 Open days and school excursions at CEITEC BUT, Brno, Czech Republic
- 2019 – 120 years of BUT anniversary, Brno, Czech Republic